

Numerical methods for shape optimal design of fluid–structure interaction problems

Johannes Haubner^{a,*}, Michael Ulbrich^b

^a University of Graz, Heinrichstr. 36, 8010, Graz, Austria

^b Technical University of Munich, Boltzmannstr. 3, 85748, Garching b. München, Germany

ARTICLE INFO

Dataset link: <https://github.com/JohannesHaubner/ShapeOpt/>

Keywords:

Fluid–structure interaction
Shape optimization
Method of mappings
Navier–Stokes equations
Saint Venant–Kirchhoff type material
FSI2 benchmark

ABSTRACT

We consider the method of mappings for performing shape optimization for unsteady fluid–structure interaction (FSI) problems. In this work, we focus on the numerical implementation. We model the optimization problem such that it takes several theoretical results into account, such as regularity requirements on the transformations and a differential geometrical point of view on the manifold of shapes. Moreover, we discretize the problem such that we can compute exact discrete gradients. This allows for the use of general purpose optimization solvers. We focus on problems derived from an FSI benchmark to validate our numerical implementation. The method is used to optimize parts of the outer boundary and the interface. The numerical simulations build on FEniCS, dolfin-adjoint and IPOPT. Moreover, as an additional theoretical result, we show that for a linear special case the adjoint attains the same structure as the forward problem but reverses the temporal flow of information.

1. Introduction

Fluid–structure interaction (FSI) is a particularly important subclass of multi-physics problems that arise frequently in applications such as wind turbines, bridges, naval architecture or biomedical applications, cf., e.g., [1]. Performing shape optimization on this class of problems is also a vivid area of research. In [2] this task is tackled from a theoretical point of view, whereas [3–11] focus on numerical approaches. In this paper, we present our numerical realization of shape optimization for an unsteady nonlinear FSI problem. Our approach is based on the method of mappings, i.e., it models shape optimization problems via domain transformations, represented by displacements, that serve as the “control” in an optimization problem with PDE constraints. As such, efficient tools and optimization algorithms can be applied that need not be tailor-made for shape optimization. The underlying transformation approach is also well aligned with the arbitrary Lagrangian–Eulerian (ALE) technique that we use to tackle the FSI problem, see Fig. 1.

1.1. Method of mappings

The different methods for performing shape optimization are closely related to the metric structure that is imposed on the set of admissible shapes. Besides the consideration of characteristic functions (which motivates, e.g., phase field approaches, cf., e.g., [12], or [13]) or distance functions [14], a metric can be defined via transformations [15]. Similarly to the FSI problem, the Lagrangian or Eulerian perspective can be chosen to work with transformations. The latter leads to the notion of shape derivatives and to level set

* Corresponding author.

E-mail addresses: johannes.haubner@uni-graz.at (J. Haubner), mulbrich@ma.tum.de (M. Ulbrich).

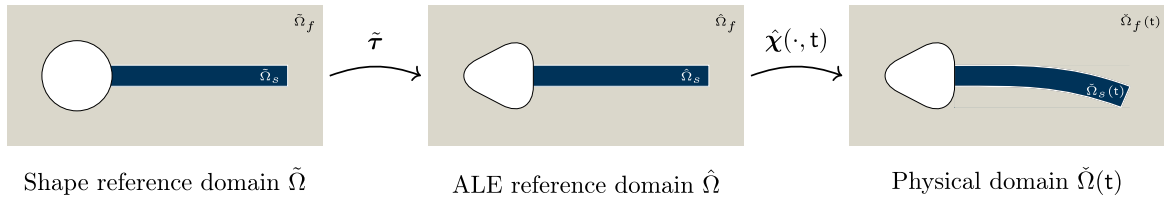


Fig. 1. Schematic illustration of the method of mappings combined with an ALE transformation.

methods. The Lagrangian perspective is called method of mappings or perturbation of the identity [15–19]. It allows for a rigorous theoretical framework for shape optimization and was already applied in fluid mechanics, see e.g. [17]. Instead of optimizing over a set of admissible shapes, a parameterization of the shape by a bi-Lipschitz homeomorphism $\tilde{\tau} : \mathbb{R}^d \rightarrow \mathbb{R}^d$ via $\hat{\Omega} = \tilde{\tau}(\tilde{\Omega})$ is used, where $\tilde{\Omega} \subset \mathbb{R}^d$ is a shape reference domain. The optimization is then performed over a set of admissible transformations. For more details we refer to the cited literature and Section 3. In this work, we apply the method of mappings to solve a shape optimization problem for unsteady nonlinear FSI.

1.1.1. Theoretical challenges

A main theoretical challenge is ensuring existence of solutions of shape optimization problems, which, in general, requires a regularization term and can be done with available optimization theory since the problem is formulated on a fixed reference domain. If a partial differential equation (PDE) constraint is involved, one crucial and technical step is proving differentiability of the state with respect to shape transformations [2,20]. In this work, we do not focus on the theoretical aspects of shape optimization of fluid–structure interaction but concentrate on the algorithmic realization.

1.1.2. Algorithmic realization

Treating, for the moment, the computation of the surface or volumetric shape functional and its derivative as black-box, our proposed algorithm takes the following form:

1. Choose a design boundary $\tilde{\Gamma}_d$ of the initial domain $\tilde{\Omega}$.
2. Choose a scalar valued quantity $\tilde{d} : \tilde{\Gamma}_d \rightarrow \mathbb{R}$ as optimization variable.
3. Apply a boundary operator $S_{\tilde{\Gamma}}$ to obtain a vector valued deformation field on the boundary.
4. Apply a suitable extension operator $S_{\tilde{\Omega}}$ to $S_{\tilde{\Gamma}}(\tilde{d})$, such that a deformation field for $\tilde{\Omega}$ is given by $S_{\tilde{\Omega}}(S_{\tilde{\Gamma}}(\tilde{d}))$. For abbreviation, we introduce $B := S_{\tilde{\Omega}} \circ S_{\tilde{\Gamma}}$.
5. Compute the value of the shape functional and its derivative at $(\text{id} + B(\tilde{d}))(\tilde{\Omega})$.
6. Use the chain rule to obtain the derivative with respect to \tilde{d} .
7. Use this within an appropriately chosen derivative-based optimization algorithm. If second order derivatives are available, also second order optimization methods can be applied.

1.1.3. Requirements on software framework

The above algorithm requires that the software framework allows for the solution of PDEs on (sub)meshes and (submeshes of) their surface meshes. Moreover, we assume that it is possible to restrict functions on the mesh to functions on submeshes and (submeshes of) their surface meshes and vice versa extend functions that live on parts of the surface appropriately (e.g. by zero) to functions on the mesh. Our implementation builds on FEniCS [21].

1.1.4. Related work

One common approach to deal with transformations based shape optimization is solving a sequence of auxiliary problems with linearized objective function based on a shape derivative to iteratively update the domain, e.g., [22–24] and references therein. In this work, solve the shape optimization problem on a fixed domain ($\tilde{\Omega}$) without linearization of the objective function. We extend results reported in [25] by a different choice of the operator B , interface optimization, and a determinant constraint, which has been theoretically substantiated in [26]. The decision for a scalar valued optimization variable is motivated by considerations on one-to-one correspondence between shapes and controls, see, e.g., [26, Remark 2.2]. In contrast to [26], where steady-state Stokes flow is considered, we tackle a challenging class of shape optimization problems that is governed by transient FSI. The theoretical foundation is presented in [2]. We note that there is still a gap between theoretical results and numerical applications, such as local-in-time vs. global-in-time results, geometrical restrictions vs. arbitrary domains, or linear hyperbolic equations vs. nonlinear elasticity.

The choice of the operator B is part of the modeling of the shape optimization problem, see, e.g., [26] and references therein. In some approaches, Steklov-Poincaré operators are used, e.g., [24], which can be incorporated into our framework via $S_{\tilde{\Gamma}}$. Other approaches involve remeshing or a multi-mesh approach [27], which can also be incorporated in our approach, e.g. via $S_{\tilde{\Omega}}$ if only the interior of the domain is remeshed. In this paper, we want to work with exact (discrete) derivatives during the optimization process. Therefore, we do not consider remeshing routines. Moreover, in order to have full control over the shape functional and its derivative, we do not consider the computation of the derivative as black box.

1.2. Fluid–structure interaction problem

We consider FSI problems for which the fluid is modeled by the unsteady incompressible Navier–Stokes equations. These are canonically formulated in the Eulerian framework, i.e., on a time-dependent physical domain $\tilde{\Omega}_f(t) \subset \mathbb{R}^d$, $d \in \{2, 3\}$, for $t \in I := (0, T)$, $T > 0$. The structure equations, however, are formulated in the Lagrangian framework, i.e., on a fixed reference domain $\hat{\Omega}_s$. The first challenge for considering the coupled problem arises from the fact that the above canonical models for the fluid and structure equations are formulated in different frameworks for which reason a precise formulation of the coupling conditions requires further effort. For FSI simulations, partitioned as well as monolithic approaches have been proposed. Partitioned methods solve the corresponding models separately and typically apply fixed point iterations to the coupling interface conditions, which can, e.g., be accelerated by Quasi-Newton techniques [28,29]. Monolithic approaches [30–35], such as arbitrary Lagrangian–Eulerian (ALE) [30,31,34] and fully Eulerian methods [31,32,35], use the same reference frame for fluid and solid. While fully Eulerian approaches use the spatial reference frame, the ALE framework is obtained by introducing an arbitrary but fixed reference domain $\hat{\Omega}_f$ such that the fluid and solid reference domains are disjoint, i.e., $\hat{\Omega}_s \cap \hat{\Omega}_f = \emptyset$, and share the interface $\hat{\Gamma}_i := \hat{\Omega}_s \cap \hat{\Omega}_f$ as part of their boundaries. To derive the fluid equations on the reference domain $\hat{\Omega}_f$, we consider an extension $\hat{\chi}(\cdot, t) : \hat{\Omega} \rightarrow \mathbb{R}^d$ of the solid transformation $\hat{\chi}_s(\cdot, t)$ to the whole reference domain $\hat{\Omega} := \hat{\Omega}_s \cup \hat{\Omega}_f \cup \hat{\Gamma}_i$ for any $t \in I$, i.e., $\hat{\chi}(\cdot, t)|_{\hat{\Omega}_s} = \hat{\chi}_s(\cdot, t)$, see Fig. 1. It can, e.g., be obtained by choosing a fully Lagrangian setting or a harmonic or biharmonic extension of the solid displacement to the fluid reference domain.

1.3. Outline

In Section 2 we present the FSI model. Some functions in the corresponding weak formulation live on parts of the domain and include boundary conditions at the interface. This, however, might not be supported by finite element toolboxes, which motivates to consider a modified weak formulation that only works with functions defined on the whole domain and boundary conditions defined on the boundary of it. Therefore, we introduce elliptic extension equations – for the pressure on the solid domain and for the solid displacement on the fluid domain – and weight them with parameters α_p and α_w . Numerical tests on the FSI2 benchmark (Section 6) show the validity of this modification if the parameters are chosen sufficiently small. Computing the derivative in an optimal control setting efficiently requires the solution of adjoint equations. For a linear special case with stationary interface, we show in Appendix that the adjoint equations of the FSI system have a similar structure as the forward equations if we eliminate the equation $\rho_s \partial_t \hat{\mathbf{w}}_s - \rho_s \hat{\mathbf{v}}_s = 0$ by defining $\hat{\mathbf{w}}_s$ via the time integral of $\hat{\mathbf{v}}_s$. Section 3 gives a comprehensive presentation of the method of mappings applied to the FSI problem. We discuss the choice of admissible shape transformations from a continuous perspective. As objective function we choose a volume formulation for the mean fluid drag. In Section 4 we present the discretization of the shape optimization for FSI via the method of mappings. We consider a continuous approach to motivate our choice of the set of admissible transformations. For the discretization of the FSI equations we build on existing approaches. In order to demonstrate the applicability of the method of mappings for FSI problems we present numerical results (Section 6) for the FSI2 benchmark using FEniCS, dolfin-adjoint and IPOPT. IPOPT works with the Euclidean inner product on \mathbb{R}^n where n denotes the number of degrees of freedom. To work with the correct inner product inherited from the continuous perspective we apply a linear transformation, see Section 5.

2. FSI model for numerical simulations

We start by deriving the coupled system. Similar techniques will be used in Section 3.1 to deduce the transformed equation on the nominal domain.

2.1. Derivation of the coupled system

We divide the fluid boundary $\partial \tilde{\Omega}_f(t) = \tilde{\Gamma}_{fD}(t) \cup \tilde{\Gamma}_{fN}(t) \cup \tilde{\Gamma}_i(t)$ into three disjoint parts on which Dirichlet (on $\tilde{\Gamma}_{fD}(t)$) or Neumann (on $\tilde{\Gamma}_{fN}(t)$) boundary conditions, or coupling conditions (on the interface $\tilde{\Gamma}_i(t)$) are imposed. The corresponding space–time cylinders are denoted by

$$\begin{aligned} \check{\Omega}_f^T &:= \bigcup_{t \in I} \tilde{\Omega}_f(t) \times \{t\}, & \check{\Sigma}_{fD}^T &:= \bigcup_{t \in I} \tilde{\Gamma}_{fD}(t) \times \{t\}, \\ \check{\Sigma}_{fN}^T &:= \bigcup_{t \in I} \tilde{\Gamma}_{fN}(t) \times \{t\}, & \check{\Sigma}_i^T &:= \bigcup_{t \in I} \tilde{\Gamma}_i(t) \times \{t\}. \end{aligned}$$

The differential equations are given by

$$\begin{aligned} \rho_f \partial_t \check{\mathbf{v}}_f + \rho_f (\check{\mathbf{v}}_f \cdot \nabla_x) \check{\mathbf{v}}_f - \operatorname{div}_x(\sigma_{f,x}(\check{\mathbf{v}}_f, \check{p}_f)) &= \rho_f \check{\mathbf{f}}_f && \text{in } \check{\Omega}_f^T, \\ \operatorname{div}_x(\check{\mathbf{v}}_f) &= 0 && \text{in } \check{\Omega}_f^T, \\ \check{\mathbf{v}}_f &= \check{\mathbf{v}}_{fD} && \text{on } \check{\Sigma}_{fD}^T, \\ \sigma_{f,x}(\check{\mathbf{v}}_f, \check{p}_f) \mathbf{n}_f &= \check{\mathbf{g}}_f && \text{on } \check{\Sigma}_{fN}^T, \end{aligned}$$

with the initial condition

$$\check{\mathbf{v}}_f(\cdot, 0) = \check{\mathbf{v}}_{0f} \quad \text{on } \check{\Omega}_f(0),$$

where $\check{\mathbf{v}}_f$ denotes the fluid velocity, \check{p}_f the pressure and $\check{\mathbf{n}}_f$ the outer unit normal vector. $\check{\mathbf{f}}_f$, $\check{\mathbf{v}}_{fD}$, $\check{\mathbf{g}}_f$ and $\check{\mathbf{v}}_{0f}$ are right-hand side, boundary and initial values. The fluid stress tensor is defined by

$$\sigma_{f,x}(\check{\mathbf{v}}_f, \check{p}_f) = \rho_f \nu_f (D_x \check{\mathbf{v}}_f + D_x \check{\mathbf{v}}_f^T) - \check{p}_f \mathbf{I},$$

with unit matrix $\mathbf{I} \in \mathbb{R}^{d \times d}$ and $D_x \check{\mathbf{v}} := (\partial_{x_j} \check{v}_i)_{i,j}$ denoting the Jacobian of $\check{\mathbf{v}}$. The parameters ρ_f and ν_f denote the fluid density and viscosity, respectively. We consider a fixed reference domain $\hat{\Omega}_s$ with disjoint Dirichlet, Neumann, and interface boundary parts $\hat{\Gamma}_{sD}$, $\hat{\Gamma}_{sN}$, and $\hat{\Gamma}_i$ such that $\partial \hat{\Omega}_s = \hat{\Gamma}_{sD} \cup \hat{\Gamma}_{sN} \cup \hat{\Gamma}_i$. The physical domain $\check{\Omega}_s(t)$ for any $t \in I$ is obtained by the transformation $\hat{\chi}_s(\cdot, t) : \hat{\Omega}_s \rightarrow \check{\Omega}_s(t)$, $\hat{\chi}_s(y, t) = y + \hat{\mathbf{w}}_s(y, t)$, where the deformation $\hat{\mathbf{w}}_s$ solves the hyperbolic equations

$$\begin{aligned} \rho_s \partial_{tt} \hat{\mathbf{w}}_s - \text{div}_y(\hat{\mathbf{F}}_{\chi_s} \Sigma_{s,y}(\hat{\mathbf{w}}_s)) &= \rho_s \hat{\mathbf{f}}_s \quad \text{in } \hat{Q}_s^T := \hat{\Omega}_s \times I, \\ \hat{\mathbf{w}}_s &= \hat{\mathbf{w}}_{sD} \quad \text{on } \hat{\Sigma}_{sD}^T := \hat{\Gamma}_{sD} \times I, \\ \hat{\mathbf{F}}_{\chi_s} \Sigma_{s,y}(\hat{\mathbf{w}}_s) \hat{\mathbf{n}}_s &= \hat{\mathbf{g}}_s \quad \text{on } \hat{\Sigma}_{sN}^T := \hat{\Gamma}_{sN} \times I, \\ \hat{\mathbf{w}}_s(\cdot, 0) &= \hat{\mathbf{w}}_{0s} \quad \text{on } \hat{\Omega}_s, \\ \partial_t \hat{\mathbf{w}}_s(\cdot, 0) &= \hat{\mathbf{w}}_1 \quad \text{on } \hat{\Omega}_s, \end{aligned}$$

and we define $\hat{\mathbf{F}}_{\chi_s} := D_y \hat{\chi}_s$. Here, ρ_s denotes the structure density and $\hat{\mathbf{f}}_s$, $\hat{\mathbf{w}}_{sD}$, $\hat{\mathbf{g}}_s$, $\hat{\mathbf{w}}_{0s}$ and $\hat{\mathbf{w}}_1$ denote right hand side, boundary and initial values. For nonlinear Saint Venant–Kirchhoff type materials the stress tensor $\Sigma_{s,y}(\hat{\mathbf{w}}_s)$ is given by

$$\Sigma_{s,y}(\hat{\mathbf{w}}_s) := \lambda_s \text{tr}(\hat{\mathbf{E}}_{\chi_s}) \mathbf{I} + 2\mu_s \hat{\mathbf{E}}_{\chi_s},$$

with $\hat{\mathbf{E}}_{\chi_s} := \frac{1}{2}(\hat{\mathbf{F}}_{\chi_s}^T \hat{\mathbf{F}}_{\chi_s} - \mathbf{I})$.

Transformation of the fluid equations with the help of $\hat{\chi}$ to the fixed reference domain $\hat{\Omega}_f$ and coupling the fluid and structure equations across the interface $\hat{\Gamma}_i$ yields the system of equations

$$\begin{aligned} \hat{J}_\chi \rho_f \partial_t \hat{\mathbf{v}}_f + \hat{J}_\chi \rho_f ((\hat{\mathbf{F}}_\chi^{-1}(\hat{\mathbf{v}}_f - \partial_t \hat{\chi})) \cdot \nabla_y) \hat{\mathbf{v}}_f \\ - \text{div}_y(\hat{J}_\chi \hat{\sigma}_f \hat{\mathbf{F}}_\chi^{-T}) &= \hat{J}_\chi \rho_f \hat{\mathbf{f}}_f \quad \text{in } \hat{Q}_f^T := \hat{\Omega}_f \times I, \\ \text{div}_y(\hat{J}_\chi \hat{\mathbf{F}}_\chi^{-1} \hat{\mathbf{v}}_f) &= 0 \quad \text{in } \hat{Q}_f^T, \\ \rho_s \partial_t \hat{\mathbf{v}}_s - \text{div}_y(\hat{J}_\chi \hat{\sigma}_s \hat{\mathbf{F}}_\chi^{-T}) &= \rho_s \hat{\mathbf{f}}_s \quad \text{in } \hat{Q}_s^T, \\ \rho_s \partial_t \hat{\mathbf{w}}_s - \rho_s \hat{\mathbf{v}}_s &= 0 \quad \text{in } \hat{Q}_s^T, \end{aligned} \tag{1}$$

with initial conditions

$$\hat{\mathbf{v}}_f(\cdot, 0) = \hat{\mathbf{v}}_{0f} \quad \text{on } \hat{\Omega}_f, \quad \hat{\mathbf{w}}_s(\cdot, 0) = \hat{\mathbf{w}}_{0s} \quad \text{on } \hat{\Omega}_s, \quad \hat{\mathbf{v}}_s(\cdot, 0) = \hat{\mathbf{w}}_1 \quad \text{on } \hat{\Omega}_s,$$

boundary conditions

$$\begin{aligned} \hat{\mathbf{v}}_f &= \hat{\mathbf{v}}_{fD} \quad \text{on } \hat{\Sigma}_{fD}^T, \quad \hat{J}_\chi \hat{\sigma}_f \hat{\mathbf{F}}_\chi^{-T} \hat{\mathbf{n}}_f = \hat{\mathbf{g}}_f \quad \text{on } \hat{\Sigma}_{fN}^T, \\ \hat{\mathbf{w}}_s &= \hat{\mathbf{w}}_{sD} \quad \text{on } \hat{\Sigma}_{sD}^T, \quad \hat{J}_\chi \hat{\sigma}_s \hat{\mathbf{F}}_\chi^{-T} \hat{\mathbf{n}}_s = \hat{\mathbf{g}}_s \quad \text{on } \hat{\Sigma}_{sN}^T, \end{aligned}$$

where $\hat{\Sigma}_{fD}^T := \hat{\Gamma}_{fD} \times I$ and $\hat{\Sigma}_{fN}^T := \hat{\Gamma}_{fN} \times I$, and additional coupling conditions

$$\begin{aligned} \hat{\mathbf{v}}_s &= \hat{\mathbf{v}}_f \quad \text{on } \hat{\Sigma}_i^T := \hat{\Gamma}_i \times I, \\ -\hat{J}_\chi \hat{\sigma}_f \hat{\mathbf{F}}_\chi^{-T} \hat{\mathbf{n}}_f &= \hat{J}_\chi \hat{\sigma}_s \hat{\mathbf{F}}_\chi^{-T} \hat{\mathbf{n}}_s \quad \text{on } \hat{\Sigma}_i^T, \end{aligned}$$

where the transformed fluid stress tensor is given by

$$\hat{\sigma}_f := \rho_f \nu_f (D_y \hat{\mathbf{v}}_f \hat{\mathbf{F}}_\chi^{-1} + \hat{\mathbf{F}}_\chi^{-T} D_y \hat{\mathbf{v}}_f^T) - \hat{p}_f \mathbf{I}.$$

Here, $\hat{\mathbf{f}}_f := \check{\mathbf{f}}_f \circ \hat{\chi}$ and $\hat{\mathbf{g}}_f$, $\hat{\mathbf{v}}_{fD}$, as well as, $\hat{\mathbf{v}}_{0f}$ are defined analogously. Moreover, $\hat{\mathbf{v}}_f = \check{\mathbf{v}}_f \circ \hat{\chi}$, $\hat{p}_f = \check{p}_f \circ \hat{\chi}$, $\hat{\sigma}_f = \sigma_{f,x}(\check{\mathbf{v}}_f, \check{p}_f) \circ \hat{\chi}$, $\hat{\sigma}_s := \hat{J}_\chi^{-1} \hat{\mathbf{F}}_\chi \Sigma_{s,y}(\hat{\mathbf{w}}_s) \hat{\mathbf{F}}_\chi^T$, where $\hat{\mathbf{F}}_\chi := D_y \hat{\chi}$ and $\hat{J}_\chi := \det(\hat{\mathbf{F}}_\chi)$, as well as, $\hat{\mathbf{v}}_s = \partial_t \hat{\mathbf{w}}_s$. In the following, we will denote coordinates on the physical domain $\check{\Omega}$ by \mathbf{x} and on the reference domain $\hat{\Omega}$ by \mathbf{y} and the subscripts of the nabla-operators indicate on which variables they act on.

Remark 1. For a function $\check{\mathbf{q}} : \check{\Omega} \times I \rightarrow \mathbb{R}^n$, $n \geq 1$, $\check{\mathbf{q}} \circ \hat{\chi}$ denotes the function that maps $(\mathbf{y}, t) \mapsto \check{\mathbf{q}}(\hat{\chi}(\mathbf{y}, t), t)$.

2.2. ALE transformation

We consider the model (1), which is fully described if the ALE transformation $\hat{\chi} : \hat{\Omega} \times I \rightarrow \bigcup_{t \in I} (\check{\Omega}(t) \times \{t\})$ is defined. There are several possibilities to choose the ALE transformation. These include, e.g., using a fully Lagrangian approach or extending

the solid displacement to the fluid domain. In theoretical investigations, the Lagrangian approach is often chosen [2,36–39], i.e., the reference domain $\hat{\Omega}$ is given by the initial domain $\hat{\Omega}(0)$ and the transformation is induced by the velocity field $\hat{\mathbf{v}}$. This has several advantages for the theoretical analysis. On the one hand, the contributions of the nonlinear term of the Navier–Stokes equations vanish on $\hat{\Omega}$. Additionally, no deformation variable on the fluid domain has to be introduced. However, it has drawbacks for numerical simulations, e.g., vortices in the flow might lead to mesh degeneration even though no solid displacement takes place. Therefore, we do not use the fully Lagrangian approach in the numerical implementation and focus on other extension techniques, which are presented below. We construct the ALE transformation by extending the solid displacement $\hat{\mathbf{w}}_s$ to the fluid reference domain, denoted by $\hat{\mathbf{w}}_f$. We define

$$\hat{\chi}(\mathbf{y}, t) := \mathbf{y} + \hat{\mathbf{w}}_f(\mathbf{y}, t)$$

for every $\mathbf{y} \in \hat{\Omega}_f$ and $t \in I$. One choice is given by the harmonic extension which, as numerical tests indicate, is prone to mesh degeneration if large mesh displacements occur [40]. Thus, we work with the biharmonic extension, cf., e.g., [40–42], of the solid displacement to the fluid domain, which is given by

$$\begin{aligned} \Delta_y^2 \hat{\mathbf{w}}_f &= 0 & \text{in } \hat{Q}_f^T, \\ \hat{\mathbf{w}}_f &= 0, \quad \nabla_y \hat{\mathbf{w}}_f \cdot \mathbf{n}_f = 0 & \text{on } \hat{\Sigma}_{fD}^T \cup \hat{\Sigma}_{fN}^T, \quad \hat{\mathbf{w}}_f = \hat{\mathbf{w}}_s, \quad \nabla_y \hat{\mathbf{w}}_f \cdot \mathbf{n}_f = 0 & \text{on } \hat{\Sigma}_i^T. \end{aligned}$$

For the solution of the discretized equations, $H^2(\hat{\Omega}_f)$ -conforming finite elements are needed. However, these elements are not necessarily available in standard finite element toolboxes. In order to circumvent this, we consider a mixed formulation of the biharmonic equation

$$\begin{aligned} -\Delta_y \hat{\mathbf{w}}_f &= \hat{\mathbf{z}}_f & \text{in } \hat{Q}_f^T, & -\Delta_y \hat{\mathbf{z}}_f = 0 & \text{in } \hat{Q}_f^T, \\ \hat{\mathbf{w}}_f &= 0 & \text{on } \hat{\Sigma}_{fD}^T \cup \hat{\Sigma}_{fN}^T, & \hat{\mathbf{w}}_f = \hat{\mathbf{w}}_s & \text{on } \hat{\Sigma}_i^T, & \nabla_y \hat{\mathbf{w}}_f \cdot \mathbf{n}_f = 0 & \text{on } \partial \hat{\Omega}_f \times I, \end{aligned}$$

see [40].

2.3. Strong ALE formulation

A full description of the FSI equations with mixed biharmonic extension of the solid deformation to the fluid domain is given by

$$\begin{aligned} \hat{J}_\chi \rho_f \partial_t \hat{\mathbf{v}}_f + \hat{J}_\chi \rho_f ((\hat{\mathbf{F}}_\chi^{-1}(\hat{\mathbf{v}}_f - \partial_t \hat{\mathbf{w}}_f)) \cdot \nabla_y) \hat{\mathbf{v}}_f \\ - \text{div}_y(\hat{J}_\chi \hat{\boldsymbol{\sigma}}_f \hat{\mathbf{F}}_\chi^{-\top}) &= \hat{J}_\chi \rho_f \hat{\mathbf{f}}_f & \text{in } \hat{Q}_f^T, \\ \text{div}_y(\hat{J}_\chi \hat{\mathbf{F}}_\chi^{-1} \hat{\mathbf{v}}_f) &= 0 & \text{in } \hat{Q}_f^T, \\ \rho_s \partial_t \hat{\mathbf{v}}_s - \text{div}_y(\hat{J}_\chi \hat{\boldsymbol{\sigma}}_s \hat{\mathbf{F}}_\chi^{-\top}) &= \rho_s \hat{\mathbf{f}}_s & \text{in } \hat{Q}_s^T, \\ \rho_s \partial_t \hat{\mathbf{w}}_s - \rho_s \hat{\mathbf{v}}_s &= 0 & \text{in } \hat{Q}_s^T, \\ -\Delta_y \hat{\mathbf{w}}_f &= \hat{\mathbf{z}}_f & \text{in } \hat{Q}_f^T, \\ -\Delta_y \hat{\mathbf{z}}_f &= 0 & \text{in } \hat{Q}_f^T, \end{aligned} \tag{2}$$

with initial and boundary conditions

$$\begin{aligned} \hat{\mathbf{v}}_f(\cdot, 0) &= \hat{\mathbf{v}}_{0f} & \text{on } \hat{\Omega}_f, & \hat{\mathbf{w}}_s(\cdot, 0) &= \hat{\mathbf{w}}_{0s} & \text{on } \hat{\Omega}_s, & \hat{\mathbf{v}}_s(\cdot, 0) &= \hat{\mathbf{v}}_1 & \text{on } \hat{\Omega}_s, \\ \hat{\mathbf{v}}_f &= \hat{\mathbf{v}}_{fD} & \text{on } \hat{\Sigma}_{fD}^T, & \hat{\mathbf{w}}_s &= \hat{\mathbf{w}}_{sD} & \text{on } \hat{\Sigma}_{sD}^T, \\ \hat{\mathbf{w}}_f &= 0 & \text{on } \hat{\Sigma}_{fD}^T \cup \hat{\Sigma}_{fN}^T, & \nabla_y \hat{\mathbf{w}}_f \cdot \mathbf{n}_f &= 0 & \text{on } \partial \hat{\Omega}_f \times I, \\ \hat{J}_\chi \hat{\boldsymbol{\sigma}}_f \hat{\mathbf{F}}_\chi^{-\top} \hat{\mathbf{n}}_f &= \hat{\mathbf{g}}_f & \text{on } \hat{\Sigma}_{fN}^T, & \hat{J}_\chi \hat{\boldsymbol{\sigma}}_s \hat{\mathbf{F}}_\chi^{-\top} \hat{\mathbf{n}}_s &= \hat{\mathbf{g}}_s & \text{on } \hat{\Sigma}_{sN}^T, \end{aligned}$$

and additional coupling conditions

$$\begin{aligned} \hat{\mathbf{v}}_s &= \hat{\mathbf{v}}_f & \text{on } \hat{\Sigma}_i^T, & \hat{\mathbf{w}}_f &= \hat{\mathbf{w}}_s & \text{on } \hat{\Sigma}_i^T, \\ -\hat{J}_\chi \hat{\boldsymbol{\sigma}}_f \hat{\mathbf{F}}_\chi^{-\top} \hat{\mathbf{n}}_f &= \hat{J}_\chi \hat{\boldsymbol{\sigma}}_s \hat{\mathbf{F}}_\chi^{-\top} \hat{\mathbf{n}}_s & \text{on } \hat{\Sigma}_i^T. \end{aligned}$$

2.4. Weak ALE formulation

We define the function spaces

$$\begin{aligned} \hat{\mathbf{V}} &= \mathbf{V}(\hat{\Omega}) \subset \{\hat{\mathbf{v}} \in H^1(\hat{\Omega})^d : \hat{\mathbf{v}}|_{\hat{\Gamma}_{fD}} = \hat{\mathbf{v}}_{fD}\}, \\ \hat{\mathbf{V}}_0 &= \mathbf{V}_0(\hat{\Omega}) \subset \{\hat{\mathbf{v}} \in H^1(\hat{\Omega})^d : \hat{\mathbf{v}}|_{\hat{\Gamma}_{fD}} = 0\}, \\ \hat{\mathbf{W}} &= \mathbf{W}(\hat{\Omega}) \subset \{\hat{\mathbf{w}} \in H^1(\hat{\Omega})^d : \hat{\mathbf{w}}|_{\hat{\Gamma}_{fD} \cup \hat{\Gamma}_{fN}} = 0, \hat{\mathbf{w}}|_{\hat{\Gamma}_{sD}} = \hat{\mathbf{w}}_{sD}\}, \\ \hat{\mathbf{W}}_{f,s,0} &:= \mathbf{W}_{f,s,0}(\hat{\Omega}) \subset \{\hat{\mathbf{w}} \in L^2(\hat{\Omega})^d : \hat{\mathbf{w}}|_{\hat{\Omega}_f} \in H^1(\hat{\Omega}_f)^d, \hat{\mathbf{w}}|_{\hat{\Omega}_s} \in H^1(\hat{\Omega}_s)^d\}, \end{aligned}$$

$$\begin{aligned}
& \hat{\mathbf{w}}|_{\hat{\Gamma}_{fD} \cup \hat{\Gamma}_{fN}} = 0, \quad \hat{\mathbf{w}}|_{\hat{\Gamma}_{sD}} = 0, \quad (\hat{\mathbf{w}}|_{\hat{\Omega}_f})|_{\hat{\Gamma}_i} = 0, \\
& \hat{\mathbf{W}}_0 = \mathbf{W}_0(\hat{\Omega}) \subset \{\hat{\mathbf{w}} \in H^1(\hat{\Omega})^d : \hat{\mathbf{w}}|_{\hat{\Gamma}_{fD} \cup \hat{\Gamma}_{fN}} = 0, \hat{\mathbf{w}}|_{\hat{\Gamma}_{sD}} = 0\}, \\
& \hat{\mathbf{Z}}_f = \mathbf{Z}_f(\hat{\Omega}) \subset H^1(\hat{\Omega}_f)^d, \\
& \hat{\mathbf{Z}}_{f,s,0} := \mathbf{Z}_{f,s,0}(\hat{\Omega}) \subset \{\hat{\mathbf{z}} \in L^2(\hat{\Omega})^d : \hat{\mathbf{z}}|_{\hat{\Omega}_f} \in H^1(\hat{\Omega}_f)^d, \hat{\mathbf{z}}|_{\hat{\Omega}_s} \in H^1(\hat{\Omega}_s)^d, (\hat{\mathbf{z}}|_{\hat{\Omega}_s})|_{\hat{\Gamma}_i} = 0\}, \\
& \hat{\mathbf{Z}} = \mathbf{Z}(\hat{\Omega}) \subset H^1(\hat{\Omega})^d, \\
& \hat{P}_f = P_f(\hat{\Omega}) \subset \{\hat{p} \in L^2(\hat{\Omega}_f) : \int_{\hat{\Omega}_f} \hat{p} dy = 0\}, \\
& \hat{P} = P(\hat{\Omega}) \subset \{\hat{p} \in L^2(\hat{\Omega}) : \int_{\hat{\Omega}} \hat{p} dy = 0\}.
\end{aligned}$$

as dense subspaces. The spaces on the right hand side allow to formally write down the weak formulation. For the weak formulation to be well-defined, higher regularity needs to be imposed. That is the reason why we defined the function spaces as subspaces. We work with dense subspaces in order to stress the fact that we do not hide additional boundary conditions by the restriction on subspaces.

In addition, let $W_{2,q}(I, \hat{\mathbf{V}}) := \{\hat{\mathbf{v}} \in L^2(I, \hat{\mathbf{V}}) : \hat{\mathbf{v}}_t \in L^q(I, \hat{\mathbf{V}}^*)\}$, where $q > 0$ and $\hat{\mathbf{V}}^*$ denotes the dual space of $\hat{\mathbf{V}}$. The weak formulation of (2) is given by:

Find $(\hat{\mathbf{v}}, \hat{p}, \hat{\mathbf{w}}, \hat{\mathbf{z}}) \in W_{2,2}(I, \hat{\mathbf{V}}) \times L^2(I, \hat{P}_f) \times W_{2,2}(I, \hat{\mathbf{W}}) \times L^2(I, \hat{\mathbf{Z}}_f)$ such that $\hat{\mathbf{v}}(\cdot, 0) = \hat{\mathbf{v}}_0$, $\hat{\mathbf{w}}(\cdot, 0) = \hat{\mathbf{w}}_0$ and

$$\begin{aligned}
\langle \hat{A}_1(\hat{\mathbf{v}}, \hat{p}, \hat{\mathbf{w}}, \hat{\mathbf{z}}), (\hat{\psi}^v, \hat{\psi}^p, \hat{\psi}^w, \hat{\psi}^z) \rangle &:= (\hat{J}_\chi \rho_f \partial_t \hat{\mathbf{v}}, \hat{\psi}^v)_{\hat{\Omega}_f} \\
&+ (\hat{J}_\chi \rho_f (\hat{\mathbf{F}}_\chi^{-1}(\hat{\mathbf{v}} - \partial_t \hat{\mathbf{w}})) \cdot \nabla_y) \hat{\mathbf{v}}, \hat{\psi}^v)_{\hat{\Omega}_f} + (\hat{J}_\chi \hat{\sigma}_f \hat{\mathbf{F}}_\chi^{-T}, D_y \hat{\psi}^v)_{\hat{\Omega}_f} - (\hat{\mathbf{g}}_f, \hat{\psi}^v)_{\hat{\Gamma}_{fN}} \\
&- (\hat{J}_\chi \rho_f \hat{\mathbf{f}}_f, \hat{\psi}^v)_{\hat{\Omega}_f} + (\rho_s \partial_t \hat{\mathbf{v}}, \hat{\psi}^v)_{\hat{\Omega}_s} + (\hat{J}_\chi \hat{\sigma}_s \hat{\mathbf{F}}_\chi^{-T}, D_y \hat{\psi}^v)_{\hat{\Omega}_s} - (\hat{\mathbf{g}}_s, \hat{\psi}^v)_{\hat{\Gamma}_{sN}} \\
&- (\hat{J}_\chi \rho_s \hat{\mathbf{f}}_s, \hat{\psi}^v)_{\hat{\Omega}_s} + (\rho_s (\partial_t \hat{\mathbf{w}} - \hat{\mathbf{v}}), \hat{\psi}^w)_{\hat{\Omega}_s} + (D_y \hat{\mathbf{z}}, D_y \hat{\psi}^w)_{\hat{\Omega}_f} + (D_y \hat{\mathbf{w}}, D_y \hat{\psi}^z)_{\hat{\Omega}_f} \\
&- (\hat{\mathbf{z}}, \hat{\psi}^z)_{\hat{\Omega}_f} + (\text{div}_y(\hat{J}_\chi \hat{\mathbf{F}}_\chi^{-1} \hat{\mathbf{v}}), \hat{\psi}^p)_{\hat{\Omega}_f} = 0,
\end{aligned}$$

for all $(\hat{\psi}^v, \hat{\psi}^p, \hat{\psi}^w, \hat{\psi}^z) \in \hat{\mathbf{V}}_0 \times \hat{P}_f \times \hat{\mathbf{W}}_{f,s,0} \times \hat{\mathbf{Z}}_f$ and a.e. $t \in I$. While the deformation (by extending the interface displacement to the fluid domain) and velocity (which was introduced as the time derivative of the deformation on the solid domain) are defined on the whole domain, the other functions are only defined on the fluid domain. Since we want to work with functions defined on the whole domain, we add the equations

$$\begin{aligned}
& \hat{p} = 0 \quad \text{in } \hat{Q}_s^T, \\
& -\Delta_y \hat{\mathbf{z}} = 0 \quad \text{in } \hat{Q}_s^T, \quad \hat{\mathbf{z}}|_{\hat{\Omega}_s} = \hat{\mathbf{z}}|_{\hat{\Omega}_f} \quad \text{on } \hat{\Sigma}_i^T, \quad (\nabla_y \hat{\mathbf{z}})|_{\hat{\Omega}_s} \cdot \hat{\mathbf{n}}_s = 0 \quad \text{on } \hat{\Sigma}_{sD}^T \cup \hat{\Sigma}_{sN}^T,
\end{aligned}$$

and consider $\hat{p} \in \hat{P}$ and $\hat{\mathbf{z}} \in \hat{\mathbf{Z}}$. This leads to the weak formulation:

Find $(\hat{\mathbf{v}}, \hat{p}, \hat{\mathbf{w}}, \hat{\mathbf{z}}) \in W_{2,2}(I, \hat{\mathbf{V}}) \times L^2(I, \hat{P}) \times W_{2,2}(I, \hat{\mathbf{W}}) \times L^2(I, \hat{\mathbf{Z}})$ such that $\hat{\mathbf{v}}(\cdot, 0) = \hat{\mathbf{v}}_0$, $\hat{\mathbf{w}}(\cdot, 0) = \hat{\mathbf{w}}_0$ and

$$\begin{aligned}
\langle \hat{A}_2(\hat{\mathbf{v}}, \hat{p}, \hat{\mathbf{w}}, \hat{\mathbf{z}}), (\hat{\psi}^v, \hat{\psi}^p, \hat{\psi}^w, \hat{\psi}^z) \rangle &:= (\hat{J}_\chi \rho_f \partial_t \hat{\mathbf{v}}, \hat{\psi}^v)_{\hat{\Omega}_f} \\
&+ (\hat{J}_\chi \rho_f (\hat{\mathbf{F}}_\chi^{-1}(\hat{\mathbf{v}} - \partial_t \hat{\mathbf{w}})) \cdot \nabla_y) \hat{\mathbf{v}}, \hat{\psi}^v)_{\hat{\Omega}_f} + (\hat{J}_\chi \hat{\sigma}_f \hat{\mathbf{F}}_\chi^{-T}, D_y \hat{\psi}^v)_{\hat{\Omega}_f} - (\hat{\mathbf{g}}_f, \hat{\psi}^v)_{\hat{\Gamma}_{fN}} \\
&- (\hat{J}_\chi \rho_f \hat{\mathbf{f}}_f, \hat{\psi}^v)_{\hat{\Omega}_f} + (\rho_s \partial_t \hat{\mathbf{v}}, \hat{\psi}^v)_{\hat{\Omega}_s} + (\hat{J}_\chi \hat{\sigma}_s \hat{\mathbf{F}}_\chi^{-T}, D_y \hat{\psi}^v)_{\hat{\Omega}_s} - (\hat{\mathbf{g}}_s, \hat{\psi}^v)_{\hat{\Gamma}_{sN}} \\
&- (\hat{J}_\chi \rho_s \hat{\mathbf{f}}_s, \hat{\psi}^v)_{\hat{\Omega}_s} + (\rho_s (\partial_t \hat{\mathbf{w}} - \hat{\mathbf{v}}), \hat{\psi}^w)_{\hat{\Omega}_s} + (D_y \hat{\mathbf{z}}, D_y \hat{\psi}^w)_{\hat{\Omega}_f} + (D_y \hat{\mathbf{w}}, D_y \hat{\psi}^z)_{\hat{\Omega}_f} \\
&- (\hat{\mathbf{z}}, \hat{\psi}^z)_{\hat{\Omega}_f} + (\text{div}_y(\hat{J}_\chi \hat{\mathbf{F}}_\chi^{-1} \hat{\mathbf{v}}), \hat{\psi}^p)_{\hat{\Omega}_f} + (\hat{p}, \hat{\psi}^p)_{\hat{\Omega}_s} + (D_y \hat{\mathbf{z}}, D_y \hat{\psi}^z)_{\hat{\Omega}_s} = 0,
\end{aligned}$$

for all $(\hat{\psi}^v, \hat{\psi}^p, \hat{\psi}^w, \hat{\psi}^z) \in \hat{\mathbf{V}}_0 \times \hat{P} \times \hat{\mathbf{W}}_{f,s,0} \times \hat{\mathbf{Z}}_{f,s,0}$ and a.e. $t \in I$. For the sake of simplicity and in order to be able to work with standard finite element function spaces for the test functions in the numerical realization, we consider a modified weak formulation by replacing $\hat{\mathbf{W}}_{f,s,0}$ with $\hat{\mathbf{W}}_0$ and $\hat{\mathbf{Z}}_{f,s,0}$ with $\hat{\mathbf{Z}}$. This change corresponds to the introduction of additional interface integrals $-((D_y \hat{\mathbf{z}})|_{\hat{\Omega}_s} \hat{\mathbf{n}}_s, \hat{\psi}^z)_{\hat{\Gamma}_i}$ and $-((D_y \hat{\mathbf{z}})|_{\hat{\Omega}_f} \hat{\mathbf{n}}_f, \hat{\psi}^w)_{\hat{\Gamma}_i}$, which can be seen by performing an integration by parts:

Find $(\hat{\mathbf{v}}, \hat{p}, \hat{\mathbf{w}}, \hat{\mathbf{z}}) \in W_{2,2}(I, \hat{\mathbf{V}}) \times L^2(I, \hat{P}) \times W_{2,2}(I, \hat{\mathbf{W}}) \times L^2(I, \hat{\mathbf{Z}})$ such that $\hat{\mathbf{v}}(\cdot, 0) = \hat{\mathbf{v}}_0$, $\hat{\mathbf{w}}(\cdot, 0) = \hat{\mathbf{w}}_0$ and

$$\begin{aligned}
\langle \hat{A}_3(\hat{\mathbf{v}}, \hat{p}, \hat{\mathbf{w}}, \hat{\mathbf{z}}), (\hat{\psi}^v, \hat{\psi}^p, \hat{\psi}^w, \hat{\psi}^z) \rangle &:= (\hat{J}_\chi \rho_f \partial_t \hat{\mathbf{v}}, \hat{\psi}^v)_{\hat{\Omega}_f} \\
&+ (\hat{J}_\chi \rho_f (\hat{\mathbf{F}}_\chi^{-1}(\hat{\mathbf{v}} - \partial_t \hat{\mathbf{w}})) \cdot \nabla_y) \hat{\mathbf{v}}, \hat{\psi}^v)_{\hat{\Omega}_f} + (\hat{J}_\chi \hat{\sigma}_f \hat{\mathbf{F}}_\chi^{-T}, D_y \hat{\psi}^v)_{\hat{\Omega}_f} - (\hat{\mathbf{g}}_f, \hat{\psi}^v)_{\hat{\Gamma}_{fN}} \\
&- (\hat{J}_\chi \rho_f \hat{\mathbf{f}}_f, \hat{\psi}^v)_{\hat{\Omega}_f} + (\rho_s \partial_t \hat{\mathbf{v}}, \hat{\psi}^v)_{\hat{\Omega}_s} + (\hat{J}_\chi \hat{\sigma}_s \hat{\mathbf{F}}_\chi^{-T}, D_y \hat{\psi}^v)_{\hat{\Omega}_s} - (\hat{\mathbf{g}}_s, \hat{\psi}^v)_{\hat{\Gamma}_{sN}} \\
&- (\hat{J}_\chi \rho_s \hat{\mathbf{f}}_s, \hat{\psi}^v)_{\hat{\Omega}_s} + (\rho_s (\partial_t \hat{\mathbf{w}} - \hat{\mathbf{v}}), \hat{\psi}^w)_{\hat{\Omega}_s} + (D_y \hat{\mathbf{z}}, D_y \hat{\psi}^w)_{\hat{\Omega}_f} + (D_y \hat{\mathbf{w}}, D_y \hat{\psi}^z)_{\hat{\Omega}_f} \\
&- (\hat{\mathbf{z}}, \hat{\psi}^z)_{\hat{\Omega}_f} + (\text{div}_y(\hat{J}_\chi \hat{\mathbf{F}}_\chi^{-1} \hat{\mathbf{v}}), \hat{\psi}^p)_{\hat{\Omega}_f} + (\hat{p}, \hat{\psi}^p)_{\hat{\Omega}_s} + (D_y \hat{\mathbf{z}}, D_y \hat{\psi}^z)_{\hat{\Omega}_s} \\
&- ((D_y \hat{\mathbf{z}})|_{\hat{\Omega}_f} \hat{\mathbf{n}}_f, \hat{\psi}^w)_{\hat{\Gamma}_i} - ((D_y \hat{\mathbf{z}})|_{\hat{\Omega}_s} \hat{\mathbf{n}}_s, \hat{\psi}^z)_{\hat{\Gamma}_i} = 0,
\end{aligned}$$

for all $(\hat{\psi}^v, \hat{\psi}^p, \hat{\psi}^w, \hat{\psi}^z) \in \hat{\mathbf{V}}_0 \times \hat{P} \times \hat{\mathbf{W}}_0 \times \hat{\mathbf{Z}}$ and a.e. $t \in I$. Working with standard finite element spaces on the whole domain to discretize the above weak formulation results in a coupling between the original equations and the added auxiliary equations since

the FEM functions cannot be arbitrarily localized (in fact, for continuous FEM nodal basis functions with a support intersecting both $\hat{\Omega}_f$ and $\hat{\Omega}_s$, the restriction to either $\hat{\Omega}_f$ or $\hat{\Omega}_s$ is not contained in the FEM space). Hence, we introduce weighting parameters $\alpha_p > 0$, $\alpha_w > 0$, $\alpha_z > 0$ and functions $\hat{t}_i \in H^1(\hat{\Omega}_i)$, which are 0 at the interface $\hat{\Gamma}_i$, 1 on $\hat{\Omega}_i \setminus B_\delta(\hat{\Gamma}_i)$ and in $(0, 1]$ on $B_\delta(\hat{\Gamma}_i) \cap \hat{\Omega}_i$, where $\delta > 0$ is sufficiently small and \bullet stands for either subscript f or s .

The weak formulation, which we consider in the numerical implementation is given by:

Find $(\hat{v}, \hat{p}, \hat{w}, \hat{z}) \in W_{2,2}(I, \hat{V}) \times L^2(I, \hat{P}) \times W_{2,2}(I, \hat{W}) \times L^2(I, \hat{Z})$ such that $\hat{v}(\cdot, 0) = \hat{v}_0$, $\hat{w}(\cdot, 0) = \hat{w}_0$ and

$$\begin{aligned} \langle \hat{A}(\hat{v}, \hat{p}, \hat{w}, \hat{z}), (\hat{\psi}^v, \hat{\psi}^p, \hat{\psi}^w, \hat{\psi}^z) \rangle &:= (\hat{J}_\chi \rho_f \partial_t \hat{v}, \hat{\psi}^v)_{\hat{\Omega}_f} \\ &+ (\hat{J}_\chi \rho_f ((\hat{F}_\chi^{-1}(\hat{v} - \partial_t \hat{w})) \cdot \nabla_y) \hat{v}, \hat{\psi}^v)_{\hat{\Omega}_f} + (\hat{J}_\chi \hat{\sigma}_f \hat{F}_\chi^{-T}, D_y \hat{\psi}^v)_{\hat{\Omega}_f} - (\hat{g}_f, \hat{\psi}^v)_{\hat{\Gamma}_{fN}} \\ &- (\hat{J}_\chi \rho_f \hat{f}_f, \hat{\psi}^v)_{\hat{\Omega}_f} + (\rho_s \partial_t \hat{v}, \hat{\psi}^v)_{\hat{\Omega}_s} + (\hat{J}_\chi \hat{\sigma}_s \hat{F}_\chi^{-T}, D_y \hat{\psi}^v)_{\hat{\Omega}_s} - (\hat{g}_s, \hat{\psi}^v)_{\hat{\Gamma}_{sN}} \\ &- (\hat{J}_\chi \rho_s \hat{f}_s, \hat{\psi}^v)_{\hat{\Omega}_s} + (\rho_s (\partial_t \hat{w} - \hat{v}), \hat{\psi}^w)_{\hat{\Omega}_s} + \alpha_w (D_y \hat{z}, D_y (\hat{t}_f \hat{\psi}^w))_{\hat{\Omega}_f} + (D_y \hat{w}, D_y \hat{\psi}^z)_{\hat{\Omega}_f} \\ &- (\hat{z}, \hat{\psi}^z)_{\hat{\Omega}_f} + (\text{div}_y (\hat{J}_\chi \hat{F}_\chi^{-1} \hat{v}), \hat{\psi}^p)_{\hat{\Omega}_f} + \alpha_p (\hat{p}, \hat{\psi}^p)_{\hat{\Omega}_f} + \alpha_z (D_y \hat{z}, D_y (\hat{t}_s \hat{\psi}^z))_{\hat{\Omega}_s} = 0, \end{aligned} \quad (3)$$

for all $(\hat{\psi}^v, \hat{\psi}^p, \hat{\psi}^w, \hat{\psi}^z) \in \hat{V}_0 \times \hat{P} \times \hat{W}_0 \times \hat{Z}$ and a.e. $t \in I$.

The corresponding formulation on the space-time cylinder reads as follows:

Find $(\hat{v}, \hat{p}, \hat{w}, \hat{z}) \in W_{2,2}(I, \hat{V}) \times L^2(I, \hat{P}) \times W_{2,2}(I, \hat{W}) \times L^2(I, \hat{Z})$ such that $\hat{v}(\cdot, 0) = \hat{v}_0$, $\hat{w}(\cdot, 0) = \hat{w}_0$ and

$$\begin{aligned} \langle \hat{A}_{QT}(\hat{v}, \hat{p}, \hat{w}, \hat{z}), (\hat{\psi}^v, \hat{\psi}^p, \hat{\psi}^w, \hat{\psi}^z) \rangle &:= (\hat{J}_\chi \rho_f \partial_t \hat{v}, \hat{\psi}^v)_{\hat{\Omega}_f^T} \\ &+ (\hat{J}_\chi \rho_f ((\hat{F}_\chi^{-1}(\hat{v} - \partial_t \hat{w})) \cdot \nabla_y) \hat{v}, \hat{\psi}^v)_{\hat{\Omega}_f^T} + (\hat{J}_\chi \hat{\sigma}_f \hat{F}_\chi^{-T}, D_y \hat{\psi}^v)_{\hat{\Omega}_f^T} - (\hat{g}_f, \hat{\psi}^v)_{\hat{\Sigma}_{fN}^T} \\ &- (\hat{J}_\chi \rho_f \hat{f}_f, \hat{\psi}^v)_{\hat{\Omega}_f^T} + (\rho_s \partial_t \hat{v}, \hat{\psi}^v)_{\hat{\Omega}_s^T} + (\hat{J}_\chi \hat{\sigma}_s \hat{F}_\chi^{-T}, D_y \hat{\psi}^v)_{\hat{\Omega}_s^T} - (\hat{g}_s, \hat{\psi}^v)_{\hat{\Sigma}_{sN}^T} \\ &- (\hat{J}_\chi \rho_s \hat{f}_s, \hat{\psi}^v)_{\hat{\Omega}_s^T} + (\rho_s (\partial_t \hat{w} - \hat{v}), \hat{\psi}^w)_{\hat{\Omega}_s^T} + \alpha_w (D_y \hat{z}, D_y (\hat{t}_f \hat{\psi}^w))_{\hat{\Omega}_f^T} \\ &+ (D_y \hat{w}, D_y \hat{\psi}^z)_{\hat{\Omega}_f^T} - (\hat{z}, \hat{\psi}^z)_{\hat{\Omega}_f^T} + \alpha_p (\hat{p}, \hat{\psi}^p)_{\hat{\Omega}_s^T} + (\text{div}_y (\hat{J}_\chi \hat{F}_\chi^{-1} \hat{v}), \hat{\psi}^p)_{\hat{\Omega}_f^T} \\ &+ \alpha_z (D_y \hat{z}, D_y (\hat{t}_s \hat{\psi}^z))_{\hat{\Omega}_s^T} = 0, \end{aligned}$$

for all $(\hat{\psi}^v, \hat{\psi}^p, \hat{\psi}^w, \hat{\psi}^z) \in W_{2,2}(I, \hat{V}_0) \times L^2(I, \hat{P}) \times W_{2,2}(I, \hat{W}_0) \times L^2(I, \hat{Z})$.

3. Model of shape optimization problem for FSI

In this section we model the shape optimization problem (Section 3.4) for the unsteady, nonlinear FSI system (3) via the method of mappings. For this purpose, we transform the FSI equations to the nominal domain (Section 3.1), choose a set of admissible transformations (Section 3.3) and an objective function (Section 3.2).

3.1. Transformation of FSI equations to nominal domain

The method of mappings is applied to shape optimization problems that are governed by the FSI equations formulated on the ALE reference domain $\hat{\Omega}$. The actual physical domain is obtained from the reference domain via the mapping $\hat{\chi}(\cdot, t) : \hat{\Omega} \rightarrow \hat{\Omega}(t)$ (which is a homeomorphism for the settings that we consider). The method of mappings applies an additional transformation $\tilde{\tau} : \hat{\Omega} \rightarrow \hat{\Omega}$, which is a bi-Lipschitz transformation from the nominal domain $\hat{\Omega}$ to $\hat{\Omega}$. In the following, we denote the coordinates of $\hat{\Omega}$ by z . Let the design part of the boundary $\tilde{\Gamma}_d$ be a subset of $(\partial \hat{\Omega} \cap \partial \hat{\Omega}_f) \cup \tilde{\Gamma}_i$. The shape reference, ALE, and physical domains and the transformations between them are illustrated in Fig. 1.

Since we want to optimize the shape of the domain and not the initial conditions or boundary conditions, we assume that the considered transformations in $\tilde{\mathcal{T}}_{ad}$ do not change these conditions. For the sake of convenience, and in correspondence with our numerical setting, we choose $\hat{g}_f = 0$ and $\hat{g}_s = 0$. Additionally, we choose the transformation such that it is equal to the identity on the support of the initial conditions (which is not a restriction in our case since the initial conditions are chosen to be 0).

For fixed $\tilde{\tau} \in \tilde{\mathcal{T}}_{ad}$, we introduce the following spaces on the shape reference domain

$$\begin{aligned} \tilde{V}_{\tilde{\tau}} &= \{\hat{v} \circ \tilde{\tau} : \hat{v} \in \hat{V}(\tilde{\tau}(\hat{\Omega}))\}, \\ \tilde{V}_{0,\tilde{\tau}} &= \{\hat{v} \circ \tilde{\tau} : \hat{v} \in \hat{V}_0(\tilde{\tau}(\hat{\Omega}))\}, \\ \tilde{W}_{\tilde{\tau}} &= \{\hat{w} \circ \tilde{\tau} : \hat{w} \in \hat{W}(\tilde{\tau}(\hat{\Omega}))\}, \\ \tilde{W}_{0,\tilde{\tau}} &= \{\hat{w} \circ \tilde{\tau} : \hat{w} \in \hat{W}_0(\tilde{\tau}(\hat{\Omega}))\}, \\ \tilde{P}_{\tilde{\tau}} &= \{\hat{p} \circ \tilde{\tau} : \hat{p} \in \hat{P}(\tilde{\tau}(\hat{\Omega}))\}, \\ \tilde{Z}_{\tilde{\tau}} &= \{\hat{z} \circ \tilde{\tau} : \hat{z} \in \hat{Z}(\tilde{\tau}(\hat{\Omega}))\}. \end{aligned}$$

Remark 2. For a function $\hat{q} : \hat{\Omega} \times I \rightarrow \mathbb{R}^n$, $n \geq 1$, $\hat{q} \circ \tilde{\tau}$ denotes the function that maps $(z, t) \mapsto \hat{q}(\tilde{\tau}(z), t)$.

The additional transformation with $\tilde{\tau}$ yields the following weak formulation on the shape reference domain $\tilde{\Omega}$. For fixed $\tilde{\tau} \in \tilde{T}_{ad}$, find $(\tilde{v}, \tilde{p}, \tilde{w}, \tilde{z}) \in W_{2,2}(I, \tilde{\mathbf{V}}_{\tilde{\tau}}) \times L^2(I, \tilde{P}_{\tilde{\tau}}) \times W_{2,2}(I, \tilde{\mathbf{W}}_{\tilde{\tau}}) \times L^2(I, \tilde{\mathbf{Z}}_{\tilde{\tau}})$ such that $\tilde{v}(\cdot, 0) = 0$, $\tilde{w}(\cdot, 0) = 0$ and

$$\begin{aligned} & \langle \tilde{A}_{\Omega}((\tilde{v}, \tilde{p}, \tilde{w}, \tilde{z}), \tilde{\tau}), (\tilde{\psi}^v, \tilde{\psi}^p, \tilde{\psi}^w, \tilde{\psi}^z) \rangle \\ & := (\det(D_z \tilde{\tau}) \tilde{J}_{\chi} \rho_f \partial_t \tilde{v}, \tilde{\psi}^v)_{\tilde{\Omega}_f} \\ & \quad + (\det(D_z \tilde{\tau}) \tilde{J}_{\chi} \rho_f (((D_z \tilde{\tau})^{-1} \tilde{\mathbf{F}}_{\chi}^{-1}(\tilde{v} - \partial_t \tilde{w})) \cdot \nabla_z) \tilde{v}, \tilde{\psi}^v)_{\tilde{\Omega}_f} \\ & \quad + (\det(D_z \tilde{\tau}) \tilde{J}_{\chi} \tilde{\sigma}_f \tilde{\mathbf{F}}_{\chi}^{-T} (D_z \tilde{\tau})^{-T}, D_z \tilde{\psi}^v)_{\tilde{\Omega}_f} - (\det(D_z \tilde{\tau}) \tilde{J}_{\chi} \rho_f \tilde{\mathbf{f}}_f, \tilde{\psi}^v)_{\tilde{\Omega}_f} \\ & \quad + (\det(D_z \tilde{\tau}) \rho_s \partial_t \tilde{v}, \tilde{\psi}^v)_{\tilde{\Omega}_s} + (\det(D_z \tilde{\tau}) \tilde{J}_{\chi} \tilde{\sigma}_s \tilde{\mathbf{F}}_{\chi}^{-T} (D_z \tilde{\tau})^{-T}, D_z \tilde{\psi}^v)_{\tilde{\Omega}_s} \\ & \quad - (\det(D_z \tilde{\tau}) \tilde{J}_{\chi} \rho_s \tilde{\mathbf{f}}_s, \tilde{\psi}^v)_{\tilde{\Omega}_s} + (\det(D_z \tilde{\tau}) \rho_s (\partial_t \tilde{w} - \tilde{v}), \tilde{\psi}^w)_{\tilde{\Omega}_s} \\ & \quad + \alpha_w (\det(D_z \tilde{\tau}) D_z \tilde{z} (D_z \tilde{\tau})^{-1} (D_z \tilde{\tau})^{-T}, D_z (\tilde{v}_f \tilde{\psi}^w))_{\tilde{\Omega}_f} \\ & \quad + (\det(D_z \tilde{\tau}) D_z \tilde{w} (D_z \tilde{\tau})^{-1} (D_z \tilde{\tau})^{-T}, D_z \tilde{\psi}^z)_{\tilde{\Omega}_f} \\ & \quad - (\det(D_z \tilde{\tau}) \tilde{z}, \tilde{\psi}^z)_{\tilde{\Omega}_f} + \alpha_p (\det(D_z \tilde{\tau}) \tilde{p}, \tilde{\psi}^p)_{\tilde{\Omega}_s} \\ & \quad + (\det(D_z \tilde{\tau}) \text{tr}(D_z (\tilde{J}_{\chi} \tilde{\mathbf{F}}_{\chi}^{-1} \tilde{v}) (D_z \tilde{\tau})^{-1}), \tilde{\psi}^p)_{\tilde{\Omega}_f} \\ & \quad + \alpha_z (\det(D_z \tilde{\tau}) D_z \tilde{z} (D_z \tilde{\tau})^{-1} (D_z \tilde{\tau})^{-T}, D_z (\tilde{v}_s \tilde{\psi}^z))_{\tilde{\Omega}_s} = 0, \end{aligned} \quad (4)$$

for all $(\tilde{\psi}^v, \tilde{\psi}^p, \tilde{\psi}^w, \tilde{\psi}^z) \in W_{2,2}(I, \tilde{\mathbf{V}}_0) \times L^2(I, \tilde{P}) \times W_{2,2}(I, \tilde{\mathbf{W}}_0) \times L^2(I, \tilde{\mathbf{Z}})$ and any $t \in I$. Moreover, $\tilde{J}_{\chi} = \det(\tilde{\mathbf{F}}_{\chi})$ and $\tilde{\mathbf{F}}_{\chi} = D_z \tilde{\chi} (D_z \tilde{\tau})^{-1}$,

$$\tilde{\sigma}_f := \rho_f \nu_f (D_z \tilde{v}_f (D_z \tilde{\tau})^{-1} \tilde{\mathbf{F}}_{\chi}^{-1} + \tilde{\mathbf{F}}_{\chi}^{-T} (D_z \tilde{\tau})^{-T} D_z \tilde{v}_f^T) - \tilde{p}_f \mathbf{I}$$

denotes the transformed fluid stress tensor and $\tilde{\sigma}_s$ the corresponding transformed solid stress tensor. For Saint Venant–Kirchhoff type material, it is given by

$$\tilde{\sigma}_s = \tilde{J}_{\chi}^{-1} \tilde{\mathbf{F}}_{\chi} (\lambda_s \text{tr}(\tilde{\mathbf{E}}_{\chi}) \mathbf{I} + 2\mu_s \tilde{\mathbf{E}}_{\chi}) \tilde{\mathbf{F}}_{\chi}^T$$

with $\tilde{\mathbf{E}}_{\chi} := \frac{1}{2} (\tilde{\mathbf{F}}_{\chi}^T \tilde{\mathbf{F}}_{\chi} - \mathbf{I})$. The corresponding operator is denoted by

$$\tilde{A}_{\Omega}(\tilde{y}, \tilde{\tau}) = 0, \quad (5)$$

where $\tilde{y} = (\tilde{v}, \tilde{p}, \tilde{w}, \tilde{z})$. Moreover, let

$$\tilde{\mathbf{Y}}_{\tilde{\tau}} := W_{2,2}(I, \tilde{\mathbf{V}}_{\tilde{\tau}}) \times L^2(I, \tilde{P}_{\tilde{\tau}}) \times W_{2,2}(I, \tilde{\mathbf{W}}_{\tilde{\tau}}) \times L^2(I, \tilde{\mathbf{Z}}_{\tilde{\tau}}).$$

3.2. Choice of objective function

As objective function, we choose the mean fluid drag which is given by

$$-\frac{1}{T} \int_0^T \int_{\tilde{I}_o(t)} \tilde{\Psi}^T \sigma_{f,x}(\tilde{v}_f, \tilde{p}_f) \tilde{\mathbf{n}}_f dS(x) dt$$

where $\tilde{I}_o(t) \subset \partial \tilde{\Omega}_f(t)$ for all $t \in [0, T]$ denotes an obstacle such that $\tilde{I}_o(t)$ and $\partial \tilde{\Omega}_f(t) \setminus \tilde{I}_o(t)$ have positive distance for all $t \in [0, T]$. Furthermore, $\tilde{\Psi} = (1, 0)^T$ and $\tilde{\mathbf{n}}_f$ denotes the outwards pointing normal vector, e.g., [17,43]. This can be reformulated as a volume integral given by

$$-\frac{1}{T} \int_0^T ((\rho_f (\partial_t \tilde{v}_f + (\tilde{v}_f \cdot \nabla_x) \tilde{v}_f), \tilde{\Psi})_{\tilde{\Omega}_f(t)} - (\tilde{p}_f, \text{div}(\tilde{\Psi}))_{\tilde{\Omega}_f(t)} + (2\nu_f \epsilon_x(\tilde{v}_f), \epsilon_x(\tilde{\Psi}))_{\tilde{\Omega}_f(t)}) dt,$$

where $\epsilon_x(\cdot) = \frac{1}{2} (D_x \cdot + (D_x \cdot)^T)$, and $\tilde{\Psi}$ is an arbitrary continuously differentiable function such that $\tilde{\Psi}|_{\tilde{I}_o} = \tilde{\Psi}$ and $\tilde{\Psi}|_{\partial \tilde{\Omega}_f \setminus \tilde{I}_o} = 0$, cf. [43–45]. The corresponding transformed formulation on the ALE domain $\tilde{\Omega}_f$ reads as

$$\begin{aligned} \hat{F}_D(\hat{y}) = & -\frac{1}{T} \int_0^T ((\hat{J}_{\chi} \rho_f (\partial_t \hat{v}_f + ((\hat{\mathbf{F}}_{\chi}^{-1}(\hat{v}_f - \partial_t \hat{z})) \cdot \nabla_y) \hat{v}_f), \hat{\Psi})_{\hat{\Omega}_f} \\ & - (\hat{J}_{\chi} \hat{p}_f, \text{tr}(D_y \hat{\Psi} \hat{\mathbf{F}}_{\chi}^{-1}))_{\hat{\Omega}_f} + (2\nu_f \hat{J}_{\chi} \epsilon_y(\hat{v}_f), \epsilon_y(\hat{\Psi}))_{\hat{\Omega}_f}) dt \end{aligned}$$

with $\hat{J}_{\chi} = \det \hat{\mathbf{F}}_{\chi}$ and $\epsilon_y(\cdot) = \frac{1}{2} ((D_y \cdot) \hat{\mathbf{F}}_{\chi}^{-1} + \hat{\mathbf{F}}_{\chi}^{-T} (D_y \cdot)^T)$, and the transformation on the shape reference domain $\tilde{\Omega}_f$ yields

$$\begin{aligned} \tilde{F}_D(\tilde{y}, \tilde{\tau}) = & -\frac{1}{T} \int_0^T ((\tilde{J}_{\chi} \det(D_z \tilde{\tau}) \rho_f (\partial_t \tilde{v}_f + ((D_z \tilde{\tau}^{-1} \tilde{\mathbf{F}}_{\chi}^{-1}(\tilde{v}_f - \partial_t \tilde{z})) \cdot \nabla_z) \tilde{v}_f), \tilde{\Psi})_{\tilde{\Omega}_f} \\ & - (\tilde{J}_{\chi} \det(D_z \tilde{\tau}) \tilde{p}, \text{tr}(D_z \tilde{\Psi} D_z \tilde{\tau}^{-1} \tilde{\mathbf{F}}_{\chi}^{-1}))_{\tilde{\Omega}_f} \\ & + (2\nu_f \tilde{J}_{\chi} \det(D_z \tilde{\tau}) \epsilon_z(\tilde{v}_f), \epsilon_z(\tilde{\Psi}))_{\tilde{\Omega}_f}) dt \end{aligned}$$

with $\epsilon_z(\cdot) = \frac{1}{2} ((D_z \cdot) D_z \tilde{\tau}^{-1} \tilde{\mathbf{F}}_{\chi}^{-1} + \tilde{\mathbf{F}}_{\chi}^{-T} D_z \tilde{\tau}^{-T} (D_z \cdot)^T)$.

3.3. Choice of admissible shape transformations

Our choice of admissible transformations is based on the following considerations:

- As already mentioned in a previous section, we choose the transformations such that they do not change initial conditions, boundary conditions or source terms, i.e., the support of the deformation $\tilde{\tau} - \text{id}_z$ is disjoint from the support of the initial conditions, boundary conditions and source terms. In case that the design part $\tilde{\Gamma}_d$ is a subset of the Dirichlet boundary, the boundary conditions are considered to be homogeneous on $\tilde{\Gamma}_d$.
- Since standard existence theory for PDEs requires Lipschitz regularity of the domain, it is natural to require the domains to be Lipschitzian during the optimization process. This can be ensured by choosing $\tilde{\Omega}$ as a Lipschitz domain and transformations $\tilde{\tau} \in W^{1,\infty}(\tilde{\Omega})^d$ close to the identity [16, Lem. 2]. The locality around the identity can be relaxed by including a determinant constraint $\det(D\tilde{\tau}) \geq \eta_{\text{ext}}$, $\eta_{\text{ext}} \in (0, 1)$, on Ω or on hold all domain $U \supset \Omega$, see [26,46]. In this work, we choose this perspective and add a penalization $\gamma_p \int_{\tilde{\Omega}} (\det(D_z \tilde{\tau}(z)) - \eta_{\text{ext}})^{-1} dz$ to the objective function, with $\gamma_p = 10^{-3}$ and $\eta_{\text{ext}} = 0.2$, and set the value of the integral to $+\infty$ (or in the numerical discretization to 10^{16}) if the constraint $\det(D_z \tilde{\tau}) - \eta_{\text{ext}} \geq 0$ is not fulfilled a.e.
- To be able to work with the same function spaces on the shape reference domain independently of the control $\tilde{\tau}$, it is desirable that the spaces for the transformed functions are isomorphic to the spaces on the transformed domain. When working in a space $\tilde{\mathbf{Y}} = \tilde{\mathbf{Y}}(\tilde{\Omega})$ on the shape reference domain, the corresponding space on the ALE reference domain is

$$\hat{\mathbf{Y}}_{\tilde{\tau}}(\hat{\Omega}) = \{\hat{\mathbf{y}} : \hat{\mathbf{y}} \circ \tilde{\tau} \in \tilde{\mathbf{Y}}\}.$$

Hence, the regularity of the space on the actual (in our case ALE reference) domain $\hat{\Omega}$ depends on the regularity of $\tilde{\tau}$ and also the regularity of $\hat{\Omega}$ depends on the regularity of $\tilde{\tau}$ and $\tilde{\Omega}$. One way to ensure well-posedness of the optimization problem is the choice of a suitable notion of solutions on $\hat{\Omega}$, a function space setting on $\hat{\Omega}$, and $\tilde{\tau}$ such that solving the PDE on the actual domain is equivalent to solving the transformed PDE on the shape reference domain and $\hat{\mathbf{Y}} = \hat{\mathbf{Y}}_{\tilde{\tau}}(\hat{\Omega})$ is independent of $\tilde{\tau}$ [2]. Thus, the regularity requirement on $\tilde{\tau}$ depends on the regularity of the state of the PDEs and $\tilde{\mathcal{T}}_{ad} \subset \tilde{\mathbf{D}}_{\Omega} \subset W^{1,\infty}(\tilde{\Omega})^d$ for a function space $\tilde{\mathbf{D}}_{\Omega}$ with sufficiently high regularity.

- Transformations that only change the interior of the domain but not the boundaries do not change the shape of the domain. To ensure a one-to-one correspondence, shape optimization problems are often considered as optimization problems on manifolds, see, e.g., [47,48], or on appropriate subsets of linear subspaces, see, e.g., [17]. In order to be in the latter setting, we consider a scalar valued quantity $\tilde{d} \in \tilde{D}_{\Gamma_d}$ on the design boundary $\tilde{\Gamma}_d$ and identify it with a shape via a transformation of the form $\text{id}_z + B(\tilde{d})$.

We work with the following operator $B : \tilde{D}_{\Gamma_d} \rightarrow \tilde{\mathbf{D}}_{\Omega}$, $\tilde{d} \mapsto \tilde{\mathbf{u}}$: We choose $\tilde{D}_{\Gamma_d} = L^2(\tilde{\Gamma}_d)$ and first solve the Laplace-Beltrami equation

$$-\text{div}_{\tilde{\Gamma}_d}(\tilde{\beta} D_{\tilde{\Gamma}_d} \tilde{\mathbf{b}}) + \tilde{\mathbf{b}} = \tilde{d} \tilde{\mathbf{n}} \text{ in } \tilde{\Gamma}_d, \quad \tilde{\mathbf{b}} = 0 \text{ on } \partial \tilde{\Gamma}_d, \quad (6)$$

where $\tilde{\beta}$ is an H^1 -regularized approximation to $\beta > 0$ in L^2 that is 1 on $\partial \tilde{\Gamma}_d$. More precisely, $\tilde{\beta}$ solves

$$-\gamma \Delta_{\tilde{\Gamma}_d} \tilde{\beta} + \tilde{\beta} = \beta \text{ in } \tilde{\Gamma}_d, \quad \tilde{\beta} = 1 \text{ on } \partial \tilde{\Gamma}_d, \quad (7)$$

where $\beta, \gamma > 0$ are given (we work with $\beta = \gamma$). In contrast to [26], $\tilde{\beta}$ is chosen via a PDE on $\tilde{\Gamma}_d$ since we consider design boundaries which have a boundary themselves. This strategy has several reasons. On the one hand, together with the regularization, it provides a control on the size of the deformation close to the boundaries of the design boundaries. On the other hand, our numerical tests have shown that an active determinant constraint penalization close to a boundary of a design boundary can impair the performance of our implementation. In order to avoid mesh degeneration, we aim for small gradients of $\tilde{\mathbf{b}}$ in the vicinity of $\partial \tilde{\Gamma}_d$. To obtain the deformation field, we solve the equation

$$\begin{aligned} -\text{div}_z(D_z \tilde{\mathbf{u}}_{\tilde{\tau}} + D_z \tilde{\mathbf{u}}_{\tilde{\tau}}^T) &= 0 \text{ in } \tilde{\Omega}, \quad \tilde{\mathbf{u}}_{\tilde{\tau}} = 0 \text{ on } (\partial \tilde{\Omega} \cup \tilde{\Gamma}_i) \setminus \tilde{\Gamma}_d, \\ (D_z \tilde{\mathbf{u}}_{\tilde{\tau}} + D_z \tilde{\mathbf{u}}_{\tilde{\tau}}^T) \tilde{\mathbf{n}} &= \tilde{\mathbf{b}} \text{ on } \tilde{\Gamma}_d, \end{aligned} \quad (8)$$

which is similarly also used in the traction method [49] or in Steklov-Poincaré type methods [24]. Note that we work with (too) smooth transformations and can therefore not obtain additional kinks. Driving β to 0 allows for the approximation of kinks, see [26].

Remark 3. The above considerations allow for a variety of possible choices for the operator B . In [25] we work with a smooth deformation direction field that is appropriately scaled by a scalar valued function that depends on \tilde{d} . Here, we consider a strategy similar to the one introduced in [26] which is not tailored towards the geometrical setting but allows for generalization to different geometries and is also applicable in 3D.

We consider sets of admissible transformations

$$\tilde{\mathcal{T}}_{ad} \subset \{\tilde{\tau} = \text{id}_z + \tilde{\mathbf{u}}_{\tilde{\tau}}, \tilde{\mathbf{u}}_{\tilde{\tau}} \in \tilde{\mathbf{U}}_{ad}\},$$

where $\tilde{\mathbf{U}}_{ad}$ is chosen such that

$$\tilde{\mathbf{U}}_{ad} \subset \{\tilde{\mathbf{u}}_{\tilde{\tau}} : \tilde{\mathbf{u}}_{\tilde{\tau}} = B(\tilde{d}), \tilde{d} \in \tilde{D}_{\Gamma_d}\}.$$

Here, $\tilde{\mathbf{U}}_{ad}$ is chosen as a closed subset. In order to ensure the bi-Lipschitzian property for all transformations corresponding to an admissible control, additional conditions have to be satisfied, e.g., $\|\tilde{d}\|_{\tilde{D}_{r_d}} \leq c$ for a sufficiently small constant $c > 0$, or a lower bound on the determinant of the gradient of the deformation.

Furthermore, it is often relevant for practical applications to have additional geometric constraints, e.g., that the volume and barycenter of the obstacle shall not change. This motivates the constraints

$$\tilde{g}_{\Omega}(\tilde{\mathbf{u}}_{\tau}) = \begin{pmatrix} \int_{\tilde{\Omega}} \det(\mathbf{I} + D_z \tilde{\mathbf{u}}_{\tau}) dz - V \\ \frac{1}{V_o} (C_1 - \int_{\tilde{\Omega}} (z + \tilde{\mathbf{u}}_{\tau})_1 \det(\mathbf{I} + D_z \tilde{\mathbf{u}}_{\tau}) dz) - B_1 \\ \vdots \\ \frac{1}{V_o} (C_d - \int_{\tilde{\Omega}} (z + \tilde{\mathbf{u}}_{\tau})_d \det(\mathbf{I} + D_z \tilde{\mathbf{u}}_{\tau}) dz) - B_d \end{pmatrix} = 0, \quad (9)$$

where \tilde{B}_o denotes the obstacle, $V_o = \int_{\tilde{B}_o} \det(\mathbf{I} + D_z \tilde{\mathbf{u}}_{\tau}) dz$ is the volume of the obstacle, $B = (B_1, \dots, B_d)$ denotes the barycenter of the obstacle, $C = (C_1, \dots, C_d)$ is the barycenter of $\tilde{B}_o \cup \tilde{\Omega}$, and V denotes the volume of $\tilde{\Omega}$. Moreover, we assumed that $\tilde{\tau}(\tilde{\Omega}) \subset (\tilde{B}_o \cup \tilde{\Omega})$, the transformed obstacle is defined by $(\tilde{B}_o \cup \tilde{\Omega}) \setminus \tilde{\tau}(\tilde{\Omega})$, and there exists $\tilde{\tau}_{ext} : \tilde{B}_o \cup \tilde{\Omega} \rightarrow \tilde{B}_o \cup \tilde{\Omega}$ that is bi-Lipschitz and such that $\tilde{\tau}_{ext}|_{\tilde{\Omega}} = \tilde{\tau}$. In the numerical implementation, we use that the volume conservation constraint implies $V_o = \int_{\tilde{B}_o} 1 dz$ and thus we use this simpler formula.

3.4. Shape optimization problem

The shape optimization problem is given by

$$\begin{aligned} \min_{\tilde{d} \in \tilde{D}_{r_d}} \quad & \tilde{J}_{\Omega}(\tilde{\mathbf{u}}_{\tau}) + \mathcal{R}(\tilde{d}) \\ \text{s.t.} \quad & \tilde{g}_{\Omega}(\tilde{\mathbf{u}}_{\tau}) = 0, \quad \tilde{\mathbf{u}}_{\tau} = \mathbf{B}(\tilde{d}), \end{aligned} \quad (10)$$

where

$$\tilde{J}_{\Omega}(\tilde{\mathbf{u}}_{\tau}) = \tilde{F}_D(\tilde{\mathbf{y}}, \text{id}_z + \tilde{\mathbf{u}}_{\tau}), \quad (11)$$

and $\tilde{\mathbf{y}}$ is the solution to the PDE $\tilde{A}_{\Omega}(\tilde{\mathbf{y}}, \text{id}_z + \tilde{\mathbf{u}}_{\tau}) = 0$, see (5). Furthermore, \mathbf{B} and \tilde{g}_{Ω} are defined in Remark 3 and \tilde{F}_D is defined in Section 3.2. Moreover, we choose

$$\mathcal{R}(\tilde{d}) = \frac{\alpha}{2} \|\tilde{d}\|_{\tilde{D}_{r_d}}^2 + \mathcal{R}_p(\tilde{d}) \quad (12)$$

with $\alpha > 0$ and $\mathcal{R}_p(\tilde{d}) = \gamma_p \int_{\tilde{\Omega}} (\det(D_z \tilde{\tau}(z)) - \eta_{ext})^{-1} dz$ being an additional penalization of a determinant constraint (see Section 3.3).

4. Discretization

In this section, we discretize the FSI system (4) in time (Section 4.1) and space (Section 4.2). To obtain a discrete formulation (Section 4.5) of the optimization problem (10), the objective function (Section 4.3) and the shape transformations (Section 4.4) have to be discretized.

4.1. Temporal discretization

Our discretization in time uses a One-Step- θ scheme, cf. [40]. For this, we divide the terms that appear in the weak formulation into different categories. The first group $\tilde{A}_T(\tilde{\mathbf{y}}, \tau)(\tilde{\psi})$ collects all terms which include time derivatives; further below, it then will be discretized in time by finite differences:

$$\begin{aligned} \tilde{A}_T(\tilde{\mathbf{y}}, \tau)(\tilde{\psi}) := & (\det(D_z \tilde{\tau}) \tilde{J}_{\chi} \rho_f (\partial_t \tilde{\mathbf{v}} - (((D_z \tilde{\tau})^{-1} \tilde{\mathbf{F}}_{\chi}^{-1} \partial_t \tilde{\mathbf{w}}) \cdot \nabla_z) \tilde{\mathbf{v}}), \tilde{\psi}^v)_{\tilde{\Omega}_f} \\ & + (\det(D_z \tilde{\tau}) \rho_s \partial_t \tilde{\mathbf{v}}, \tilde{\psi}^v)_{\tilde{\Omega}_s} + (\det(D_z \tilde{\tau}) \rho_s \partial_t \tilde{\mathbf{w}}, \tilde{\psi}^w)_{\tilde{\Omega}_s}. \end{aligned}$$

The group $\tilde{A}_I(\tilde{\mathbf{y}}, \tau)(\tilde{\psi})$ gathers all implicit terms, i.e., all terms that should be fulfilled exactly by the new iterate such as the incompressibility condition for the fluid:

$$\begin{aligned} \tilde{A}_I(\tilde{\mathbf{y}}, \tau)(\tilde{\psi}) := & (\det(D_z \tilde{\tau}) \text{tr}(D_z (\tilde{J}_{\chi} \tilde{\mathbf{F}}_{\chi}^{-1} \tilde{\mathbf{v}}) (D_z \tilde{\tau})^{-1}), \tilde{\psi}^p)_{\tilde{\Omega}_f} \\ & + \alpha_p (\det(D_z \tilde{\tau}) \tilde{p}, \tilde{\psi}^p)_{\tilde{\Omega}_s} - (\det(D_z \tilde{\tau}) \tilde{\mathbf{z}}, \tilde{\psi}^z)_{\tilde{\Omega}_f} \\ & + (\det(D_z \tilde{\tau}) D_z \tilde{\mathbf{w}} (D_z \tilde{\tau})^{-1} (D_z \tilde{\tau})^{-\top}, D_z \tilde{\psi}^z)_{\tilde{\Omega}_f} \\ & + \alpha_z (\det(D_z \tilde{\tau}) D_z \tilde{\mathbf{z}} (D_z \tilde{\tau})^{-1} (D_z \tilde{\tau})^{-\top}, D_z (\tilde{\tau}_s \tilde{\psi}^z))_{\tilde{\Omega}_s}. \end{aligned}$$

Another group $\tilde{A}_P(\tilde{\mathbf{y}}, \tau)(\tilde{\psi})$, which is also treated implicitly, collects the pressure terms:

$$\tilde{A}_P(\tilde{\mathbf{y}}, \tau)(\tilde{\psi}) := (\det(D_z \tilde{\tau}) \tilde{J}_{\chi} \tilde{\sigma}_{f,p} \tilde{\mathbf{F}}_{\chi}^{-\top} (D_z \tilde{\tau})^{-\top}, D_z \tilde{\psi}^v)_{\tilde{\Omega}_f},$$

where $\tilde{\sigma}_{f,p} = -\tilde{p}\mathbf{I}$. This can be motivated by the fact that the pressure serves as Lagrange multiplier for the incompressibility condition. The remaining terms are collected in the fourth group $\tilde{A}_E(\tilde{\mathbf{y}}, \tilde{\boldsymbol{\tau}})(\tilde{\boldsymbol{\psi}})$:

$$\begin{aligned}\tilde{A}_E(\tilde{\mathbf{y}}, \tilde{\boldsymbol{\tau}})(\tilde{\boldsymbol{\psi}}) := & (\det(D_z \tilde{\boldsymbol{\tau}}) \tilde{J}_{\chi} \rho_f (((D_z \tilde{\boldsymbol{\tau}})^{-1} \tilde{\mathbf{F}}_{\chi}^{-1} \tilde{\mathbf{v}}) \cdot \nabla_z) \tilde{\mathbf{v}}, \tilde{\boldsymbol{\psi}}^v)_{\tilde{\Omega}_f} \\ & + \alpha_w (\det(D_z \tilde{\boldsymbol{\tau}}) D_z \tilde{\mathbf{z}} (D_z \tilde{\boldsymbol{\tau}})^{-1} (D_z \tilde{\boldsymbol{\tau}})^{-\top}, D_z (\tilde{\mathbf{f}}_f \tilde{\boldsymbol{\psi}}^w))_{\tilde{\Omega}_f} \\ & + (\det(D_z \tilde{\boldsymbol{\tau}}) \tilde{J}_{\chi} \tilde{\sigma}_{f,v} \tilde{\mathbf{F}}_{\chi}^{-\top} (D_z \tilde{\boldsymbol{\tau}})^{-\top}, D_z \tilde{\boldsymbol{\psi}}^v)_{\tilde{\Omega}_f} \\ & + (\det(D_z \tilde{\boldsymbol{\tau}}) \tilde{J}_{\chi} \tilde{\sigma}_s \tilde{\mathbf{F}}_{\chi}^{-\top} (D_z \tilde{\boldsymbol{\tau}})^{-\top}, D_z \tilde{\boldsymbol{\psi}}^v)_{\tilde{\Omega}_s} \\ & - (\det(D_z \tilde{\boldsymbol{\tau}}) \tilde{J}_{\chi} \rho_f \tilde{\mathbf{f}}_f, \tilde{\boldsymbol{\psi}}^v)_{\tilde{\Omega}_f} - (\det(D_z \tilde{\boldsymbol{\tau}}) \tilde{J}_{\chi} \rho_s \tilde{\mathbf{f}}_s, \tilde{\boldsymbol{\psi}}^v)_{\tilde{\Omega}_s} \\ & - (\det(D_z \tilde{\boldsymbol{\tau}}) \rho_s \tilde{\mathbf{v}}, \tilde{\boldsymbol{\psi}}^w)_{\tilde{\Omega}_s},\end{aligned}$$

where $\tilde{\sigma}_{f,v} = \tilde{\sigma}_f - \tilde{\sigma}_{f,p}$. The time-stepping scheme can thus be summarized as follows. Let a transformation $\tilde{\boldsymbol{\tau}}$ be given, $N \in \mathbb{N}$, $0 = t_0 < t_1 < \dots < t_N = T$ be a discretization of $\bar{I} = [0, T]$ and $\theta \in [0, 1]$. Let, for $j \in \{1, 2, \dots, N\}$, $\tilde{\mathbf{y}}^{j-1}$ be the solution at the time t_{j-1} and the time step size be constant, i.e., $k := k_j = t_j - t_{j-1}$ for all $n \in \{1, \dots, N\}$. Then, the solution at t_j is computed by:

Find $\tilde{\mathbf{y}}^j \in \tilde{\mathbf{V}}_{\tilde{\boldsymbol{\tau}}} \times \tilde{\mathbf{P}}_{\tilde{\boldsymbol{\tau}}} \times \tilde{\mathbf{W}}_{\tilde{\boldsymbol{\tau}}} \times \tilde{\mathbf{Z}}_{\tilde{\boldsymbol{\tau}}}$ such that

$$\begin{aligned}\tilde{A}_T^{j,k}(\tilde{\mathbf{y}}^j, \tilde{\boldsymbol{\tau}})(\tilde{\boldsymbol{\psi}}) + \theta \tilde{A}_E(\tilde{\mathbf{y}}^j, \tilde{\boldsymbol{\tau}})(\tilde{\boldsymbol{\psi}}) + \tilde{A}_P(\tilde{\mathbf{y}}^j, \tilde{\boldsymbol{\tau}})(\tilde{\boldsymbol{\psi}}) + \tilde{A}_I(\tilde{\mathbf{y}}^j, \tilde{\boldsymbol{\tau}})(\tilde{\boldsymbol{\psi}}) \\ = -(1 - \theta) \tilde{A}_E(\tilde{\mathbf{y}}^{j-1}, \tilde{\boldsymbol{\tau}})(\tilde{\boldsymbol{\psi}}),\end{aligned}$$

for all test functions $\tilde{\boldsymbol{\psi}} \in \tilde{\mathbf{V}}_0 \times \tilde{\mathbf{P}} \times \tilde{\mathbf{W}}_0 \times \tilde{\mathbf{Z}}$. Here, $\tilde{A}_T^{j,k}(\tilde{\mathbf{y}}, \tilde{\boldsymbol{\tau}})(\tilde{\boldsymbol{\psi}})$ is defined as the approximation of $\tilde{A}_T(\tilde{\mathbf{y}}, \tilde{\boldsymbol{\tau}})(\tilde{\boldsymbol{\psi}})$ given by

$$\begin{aligned}\tilde{A}_T^{j,k}(\tilde{\mathbf{y}}, \tilde{\boldsymbol{\tau}})(\tilde{\boldsymbol{\psi}}) \\ := \frac{1}{k} (\det(D_z \tilde{\boldsymbol{\tau}}) \tilde{J}_{\chi}^{j,\theta} \rho_f ((\tilde{\mathbf{v}} - \tilde{\mathbf{v}}^{j-1}) - (((D_z \tilde{\boldsymbol{\tau}})^{-1} \tilde{\mathbf{F}}_{\chi}^{-1} (\tilde{\mathbf{w}} - \tilde{\mathbf{w}}^{j-1}) \cdot \nabla_z) \tilde{\mathbf{v}}), \tilde{\boldsymbol{\psi}}^v)_{\tilde{\Omega}_f} \\ + \frac{1}{k} (\det(D_z \tilde{\boldsymbol{\tau}}) \rho_s (\tilde{\mathbf{v}} - \tilde{\mathbf{v}}^{j-1}), \tilde{\boldsymbol{\psi}}^v)_{\tilde{\Omega}_s} + \frac{1}{k} (\det(D_z \tilde{\boldsymbol{\tau}}) \rho_s (\tilde{\mathbf{w}} - \tilde{\mathbf{w}}^{j-1}), \tilde{\boldsymbol{\psi}}^w)_{\tilde{\Omega}_s},\end{aligned}$$

where $\tilde{J}_{\chi}^{j,\theta} := \theta \tilde{J}_{\chi} + (1 - \theta) \tilde{J}_{\chi}^{j-1}$ and the time derivatives are approximated by backward difference quotients.

The parameter θ is chosen as $\theta = \frac{1}{2} + \frac{1}{2}k$, which corresponds to a shifted Crank–Nicolson scheme. By this choice one obtains second order accuracy in time and additionally recovers global stability [50, Sec. 5.3]. The latter is important for stable behavior for long-term computations and not guaranteed by the standard Crank–Nicolson scheme, see [51].

4.2. Spatial discretization

For the spatial discretization, we use a triangulation \mathcal{T}_h of the domain $\tilde{\Omega}$ with 4262 vertices and 8225 cells K . For the sake of clarity, and since we focus on presenting the main ideas, we denote the discretized domains also by $\tilde{\Omega}$, $\tilde{\Omega}_f$ and $\tilde{\Omega}_s$. Moreover, we also do not write the subscript h for discretized boundaries, e.g., we denote $\tilde{\Gamma}_{d,h}$ by $\tilde{\Gamma}_d$. In order to have a stable discretization of the Navier–Stokes part of the FSI equations, we choose lowest order Taylor–Hood elements $(\tilde{\mathbf{v}}_h, \tilde{p}_h) \in (\mathcal{P}^2(\mathcal{T}_h)^d, \mathcal{P}^1(\mathcal{T}_h))$, where

$$\mathcal{P}^l(\mathcal{T}_h)^m := \{\tilde{\mathbf{v}}_h \in \mathcal{C}(\bigcup_{K \in \mathcal{T}_h} K)^m : \tilde{\mathbf{v}}_h|_K \text{ is a polynomial of degree } l, \forall K \in \mathcal{T}_h\}$$

for $l \geq 0$ and $m \in \mathbb{N}$, i.e., $\tilde{\mathbf{v}}_h$ is continuous and element-wise quadratic and \tilde{p}_h is continuous and linear on every element. Since $\tilde{\mathbf{v}}_h$ is equal to the temporal derivative of $\tilde{\mathbf{w}}_h$ on $\tilde{\Omega}_s$, $\tilde{\mathbf{w}}_h$ is chosen such that it has the same degrees of freedom as $\tilde{\mathbf{v}}_h$. Therefore, we choose $(\tilde{\mathbf{w}}_h, \tilde{\mathbf{z}}_h) \in (\mathcal{P}^2(\mathcal{T}_h)^d, \mathcal{P}^2(\mathcal{T}_h)^d)$. More precisely, the spaces $\tilde{\mathbf{V}}_{\tilde{\boldsymbol{\tau}}}$, $\tilde{\mathbf{V}}_{0,\tilde{\boldsymbol{\tau}}}$, $\tilde{\mathbf{W}}_{\tilde{\boldsymbol{\tau}}}$, $\tilde{\mathbf{W}}_{0,\tilde{\boldsymbol{\tau}}}$, $\tilde{\mathbf{Z}}_{\tilde{\boldsymbol{\tau}}}$, and $\tilde{\mathbf{P}}_{\tilde{\boldsymbol{\tau}}}$ are approximated by the spaces

$$\begin{aligned}\tilde{\mathbf{V}}_h &= \{\tilde{\mathbf{v}}_h \in \mathcal{P}^2(\mathcal{T}_h)^d : \tilde{\mathbf{v}}_h|_{\tilde{\Gamma}_{fD}} = \tilde{\mathbf{v}}_f|_{D,h}\}, \\ \tilde{\mathbf{V}}_{0,h} &= \{\tilde{\mathbf{v}}_h \in \mathcal{P}^2(\mathcal{T}_h)^d : \tilde{\mathbf{v}}_h|_{\tilde{\Gamma}_{fD}} = 0\}, \\ \tilde{\mathbf{W}}_h &= \{\tilde{\mathbf{w}}_h \in \mathcal{P}^2(\mathcal{T}_h)^d : \tilde{\mathbf{w}}_h|_{\tilde{\Gamma}_{fD} \cup \tilde{\Gamma}_{fN}} = 0, \tilde{\mathbf{w}}_h|_{\tilde{\Gamma}_{sD}} = \tilde{\mathbf{w}}_s|_{D,h}\}, \\ \tilde{\mathbf{W}}_{0,h} &= \{\tilde{\mathbf{w}}_h \in \mathcal{P}^2(\mathcal{T}_h)^d : \tilde{\mathbf{w}}_h|_{\tilde{\Gamma}_{fD} \cup \tilde{\Gamma}_{fN}} = 0, \tilde{\mathbf{w}}_h|_{\tilde{\Gamma}_{sD}} = 0\}, \\ \tilde{\mathbf{Z}}_h &= \mathcal{P}^2(\mathcal{T}_h)^d, \\ \tilde{\mathbf{P}}_h &= \mathcal{P}^1(\mathcal{T}_h).\end{aligned}$$

4.3. Discretization of objective function

The spatial discretization of the objective function is determined by the discretization of the state of the FSI problem. To discretize the appearing time derivative terms, we use a finite difference scheme, more precisely, the time derivative $\partial_t \tilde{\mathbf{v}}_h(t_j)$ is approximated by $(t_j - t_{j-1})^{-1}(\tilde{\mathbf{v}}_h(t_j) - \tilde{\mathbf{v}}_h(t_{j-1}))$. The time integral is approximated using the trapezoidal rule.

4.4. Discretization of shape transformations

In Remark 3, it is motivated that the choice of admissible shape transformations is delicate and requires available existence and regularity theory for the governing PDEs. However, existence and regularity theory for FSI systems is only available for special cases and under additional restrictions or assumptions. In particular, there are no theoretical results concerning existence and regularity of solutions available for the model (2). Thus, we restrict the considerations to the discretized problem. Here, the main requirements for choosing admissible shape transformations reduce to ensure the following:

- The source term, the boundary and initial conditions remain untouched by admissible shape transformations.
- The transformed triangulation $\tilde{\tau}_h(\mathcal{T}_h)$ is the discretization of a Lipschitz domain, which means that mesh degeneration is prevented. This is a delicate task that gained attention in several publications. In the context of shape optimization see, e.g., [52] and the references therein, in the context of ALE transformations see, e.g., [53–55]. In this work, we tackle it by choosing the set of admissible transformations carefully from a continuous perspective, see Section 3.3.
- The space $\tilde{\mathbf{Y}}_h(\mathcal{T}_h) \circ \tilde{\tau}_h$ is isomorphic to $\tilde{\mathbf{Y}}_h(\tilde{\tau}_h(\mathcal{T}_h))$ for all $\tilde{\tau}_h \in \tilde{\mathcal{T}}_{ad,h}$, where $\tilde{\mathbf{Y}}_h$ denotes the discrete state space and $\tilde{\mathcal{T}}_{ad,h}$ the discrete set of admissible transformations. To do so, we choose $\tilde{\mathcal{T}}_{ad,h} \subset \mathcal{P}^1(\mathcal{T}_h)$.
- There is a one-to-one-correspondence between transformations and shapes. Analogously to the continuous case, we choose a scalar valued variable $\tilde{d}_h \in \tilde{D}_{\Gamma_d,h}$, where $\tilde{D}_{\Gamma_d,h}$ denotes the space of piecewise linear functions on Γ_d , in addition, require that $\tilde{\tau}_h$ is equal to the identity on Ω_s and consider the discretized version of the operator B presented in Section 3.3.

4.5. Discretized version of the shape optimization problem

Let $\mathbf{d} \in \mathbb{R}^n$ denote the vector that represents \tilde{d}_h via

$$\tilde{d}_h = \Psi(\mathbf{d}) := \sum_{i=1}^n \mathbf{d}_i \Phi_i, \quad (13)$$

where $\{\Phi_i : i = 1, \dots, n\}$ is the nodal basis of the piecewise linear continuous elements on \tilde{D}_{Γ_d} . Moreover, let $B_h : \tilde{D}_{\Gamma_d,h} \rightarrow \mathcal{P}^1(\mathcal{T}_h)^d$, $\tilde{d}_h \mapsto \tilde{\mathbf{u}}_{r,h}$, be the discretization of B which is obtained by solving the discretizations of (6) and (8), and \tilde{j}_Ω and \tilde{g}_Ω be defined as in Section 3.4. The discretized shape optimization problem then is

$$\min_{\mathbf{d} \in \mathbb{R}^n} f(\mathbf{d}) + \frac{\alpha}{2} \mathbf{d}^\top \mathbf{S} \mathbf{d} \quad \text{s.t.} \quad g(\mathbf{d}) = 0, \quad (14)$$

where

$$\mathbf{S}_{i,j} = (\Phi_i, \Phi_j)_{\tilde{D}_{\Gamma_d,h}} = (\Phi_i, \Phi_j)_{L^2(\tilde{\Gamma}_d)}. \quad (15)$$

The vector \mathbf{d} characterizes a transformation via the following chain of compositions

$$\mathbf{d} \xrightarrow{\Psi} \tilde{d}_h \xrightarrow{B_h} \tilde{\mathbf{u}}_{r,h} \xrightarrow{\text{id}_z + \cdot} \tilde{\tau}_h.$$

The objective is defined by $f(\mathbf{d}) := \tilde{j}_\Omega(\tilde{\mathbf{u}}_{r,h}) + \mathcal{R}_p(\tilde{d}_h)$ and $g(\mathbf{d}) = \tilde{g}_\Omega(\tilde{\mathbf{u}}_{r,h})$, where $\tilde{\mathbf{u}}_{r,h} = \tilde{\mathbf{u}}_{r,h}(\mathbf{d})$, cf. (10).

5. Numerical implementation

The numerical tests¹ presented here are implemented in FEniCS [21], a collection of free software for the automated solution of PDEs. For the computation of the gradients the additional package dolfin-adjoint [56] is used, which provides the automated differentiation of the reduced cost functional based on adjoint computations on the discrete system. For large scale computations, the simulation needs to be based on a checkpointing strategy [57], meaning that, to save memory, the forward solution is not saved for every time-step but only at several checkpoints. In order to solve the backwards equations, the forward equation is resolved starting from the closest checkpoints and then adjoint timesteps are made over this strip of recomputed states. In this paper, we solve the PDE system that we transformed by hand to $\tilde{\Omega}$. We mention, however, that there exist shape differentiation tools that automate this and build on the same transformation idea [58,59].

Many existing implementations of optimization methods, such as IPOPT, work with the Euclidean inner product. Therefore, handling the discretized optimization problem (14) directly to IPOPT leads to a loss of information since it is no longer taken into account that \tilde{d}_h is the discretization of a function in a specific function space. Since we have $\tilde{d}_h(z) := \sum_{i=1}^n \mathbf{d}_i \Phi_i(z)$, the correct inner product of vectors \mathbf{d}^1 and \mathbf{d}^2 is thus given by $(\mathbf{d}^1)^\top \mathbf{S}(\mathbf{d}^2)$, where \mathbf{S} is defined in (15). Working on the space of transformed coordinates

$$\tilde{\mathbf{d}} = \tilde{\mathbf{S}} \mathbf{d}, \quad (16)$$

¹ The source code is available at <https://github.com/JohannesHaubner/ShapeOpt/>.

where $\check{\mathbf{S}}$ is chosen such that $\check{\mathbf{S}}^\top \check{\mathbf{S}} = \mathbf{S}$, e.g., $\check{\mathbf{S}} = \mathbf{S}^{\frac{1}{2}}$ (which is impractical if the size of \mathbf{S} is large) or obtained by a (sparse) Cholesky decomposition, takes the above considerations into account. We pass the following functions to IPOPT

$$\check{f} : \mathbb{R}^n \rightarrow \mathbb{R}, \quad \check{\mathbf{d}} \mapsto f(\check{\mathbf{S}}^{-1} \check{\mathbf{d}}) + \frac{\alpha}{2} \check{\mathbf{d}}^\top \check{\mathbf{d}}, \quad (17)$$

as well as, $\nabla \check{f} : \mathbb{R}^n \rightarrow \mathbb{R}^n$, $\check{\mathbf{d}} \mapsto \check{\mathbf{S}}^{-\top} \nabla f(\check{\mathbf{S}}^{-1} \check{\mathbf{d}}) + \alpha \check{\mathbf{d}}$. This has several advantages in the numerical solution process of the optimization problem. Performing a steepest descent method with step size 1 for the function \check{f} results in $\check{\mathbf{d}}^k = \check{\mathbf{S}}^{-1} \mathbf{d}^k$ and

$$\mathbf{d}^{k+1} = \check{\mathbf{S}}^{-1} \check{\mathbf{d}}^{k+1} = \check{\mathbf{S}}^{-1} (\check{\mathbf{d}}^k - (\check{\mathbf{S}}^{-\top} \nabla f(\check{\mathbf{S}}^{-1} \check{\mathbf{d}}^k) + \alpha \check{\mathbf{d}}^k)) = \mathbf{d}^k - (\mathbf{S}^{-1} \nabla f(\mathbf{d}^k) + \alpha \mathbf{d}^k),$$

i.e., a steepest descent method for $f(\cdot) + \frac{\alpha}{2} \mathbf{S}(\cdot)^\top \mathbf{S}(\cdot)$ using the Riesz representation of the derivative, which is given by $\mathbf{S}^{-1} \nabla f(\cdot) + \alpha(\cdot)$. In [60] it is shown that this leads to mesh-independent convergence rates for some examples. This is also expected for other optimization algorithms. Hence, we consider the optimization problem

$$\min_{\check{\mathbf{d}} \in \mathbb{R}^n} f(\check{\mathbf{S}}^{-1} \check{\mathbf{d}}) + \frac{\alpha}{2} \check{\mathbf{d}}^\top \check{\mathbf{d}} \quad \text{s.t.} \quad \check{g}(\check{\mathbf{d}}) = 0,$$

where

$$\check{g}(\check{\mathbf{d}}) = g(\check{\mathbf{S}}^{-1} \check{\mathbf{d}}). \quad (18)$$

Alternatively, one could apply an algorithm which directly works with the correct inner product.

We remark that, in our case, \tilde{D}_{r_d} is chosen as $L^2(\tilde{\Gamma}_d)$, thus \mathbf{S} is a mass matrix that is spectrally equivalent to the lumped mass matrix, which is diagonal. Therefore, our change of variables has a similar effect as suitably rescaling the variables. But if smoother or less smooth transformations would be desired, then \tilde{D}_{r_d} could be chosen as some other space, e.g., $H^s(\tilde{\Gamma}_d)$, with $s > 0$ (or < 0) corresponding to more (or less) smoothness.

Summarizing the above derivations, our numerical implementation is based on the following steps:

1. The optimization variable is $\check{\mathbf{d}} \in \mathbb{R}^n$, where n denotes the number of interior vertices of the discretized design boundary.
2. In a first step, $\check{\mathbf{d}}$ is mapped to $\mathbf{d} \in \mathbb{R}^n$ by computing $\check{\mathbf{S}}^{-1} \check{\mathbf{d}}$ (see (16)).
3. The vector \mathbf{d} is identified with a function \tilde{d}_h on the discretized design boundary via (13).
4. Applying the operator B_h , which corresponds to solving the discretized versions of (6) and (8) using FEniCS (see Section 4.5), yields a deformation field $\tilde{\mathbf{u}}_{r,h}$ and the corresponding transformation $\tilde{\tau}_h$.
5. Solving the transformed FSI system with FEniCS as described in Sections 4.1 and 4.2 yields the state $\tilde{\mathbf{y}}_h$.
6. Using $\tilde{\mathbf{y}}_h$ and $\tilde{\mathbf{u}}_{r,h}$, the objective function is evaluated, which is the discretization of $\tilde{J}_\Omega(\tilde{\mathbf{u}}_{r,h}) + \mathcal{R}(\tilde{d}_h) = \tilde{J}_\Omega(\tilde{\mathbf{u}}_{r,h}) + \frac{\alpha}{2} \|\tilde{d}_h\|_{\tilde{D}_{r_d}}^2 + \mathcal{R}_p(\tilde{d}_h) = \tilde{F}_D(\tilde{\mathbf{y}}_h, \text{id}_z + \tilde{\mathbf{u}}_{r,h}) + \frac{\alpha}{2} \|\tilde{d}_h\|_{\tilde{D}_{r_d}}^2 + \mathcal{R}_p(\tilde{d}_h)$ (see (11) and (12)) that we denote by $\check{f}(\check{\mathbf{d}}) = f(\mathbf{d}) + \frac{\alpha}{2} \mathbf{d}^\top \mathbf{d}$ (see (16), (17)).
7. The objective function \check{f} and its derivative (which we obtain by using the chain rule and the algorithmic differentiation framework dolfin-adjoint) and the constraints \check{g} (see (9) and (18)) and its Jacobian are handed over to the general purpose optimization solver IPOPT.

The software package IPOPT [61] is linked against HSL [62] and uses a limited-memory BFGS approximation for the Hessian. The solutions of PDE systems are done with the (nonlinear) solver of FEniCS, which uses the parallel direct LU solver MUMPS [63] for linear solves.

6. Numerical results

In this section, we present numerical results based on the FSI2 benchmark (Section 6.1). Moreover, we show results for different settings by altering the geometry and objective function (Section 6.2.1).

6.1. FSI2 benchmark

We build the validation of our numerical implementation on the FSI2 benchmark, which was proposed in [64]. This benchmark considers the coupling of the Navier–Stokes equations and Saint Venant–Kirchhoff type material equations in a two-dimensional rectangular domain of length $l = 2.5$ and height $h = 0.41$, the bottom left corner of which is located at the origin $(0, 0)^\top$. On the left boundary $\tilde{\Gamma}_{fDi}$ we have a parabolic inflow given by

$$\tilde{\mathbf{v}}_{fD}((0, z_2)^\top, t) = \begin{cases} (3\bar{v}h^{-2}z_2(h - z_2)(1 - \cos(\frac{\pi}{2}t)), 0)^\top & \text{if } t < 2.0, \\ (6\bar{v}h^{-2}z_2(h - z_2), 0)^\top & \text{otherwise,} \end{cases}$$

with mean inflow velocity \bar{v} . No-slip conditions on the bottom and top $\tilde{\Gamma}_{fD0}$ and do-nothing boundary conditions on the right boundary $\tilde{\Gamma}_{fN}$, i.e., $\tilde{\mathbf{g}}_f = 0$, are imposed. In this pipe, there is a circular obstacle with radius $r = 0.05$ centered at $(0.2, 0.2)$ to which an elastic beam of length 0.4 and width 0.02 is attached as illustrated in Fig. 2. On $\tilde{\Gamma}_{fDc}$, the part of the circular obstacle that is part of the fluid boundary, homogeneous Dirichlet boundary conditions are imposed on the fluid velocity and solid displacement. The initial conditions are set to 0. Thus, the fluid–structure system is completely determined by the parameters $\rho_s = 1 \cdot 10^4$, $\lambda_s = 2 \cdot 10^6$, $\mu_s = 5 \cdot 10^5$, $\rho_f = 1 \cdot 10^3$, $\nu_f = 1 \cdot 10^{-3}$, $\bar{v} = 1$ and $\alpha_p = \alpha_w = 1 \cdot 10^{-9}$. Details on the implementation are given in the previous sections. As time horizon for the optimization of the mean drag we choose $T = 15$ s. Given a design boundary (or interface) $\tilde{\Gamma}_d$, we want to optimize the shape of $\tilde{\Omega}$ such that the fluid drag is minimized.

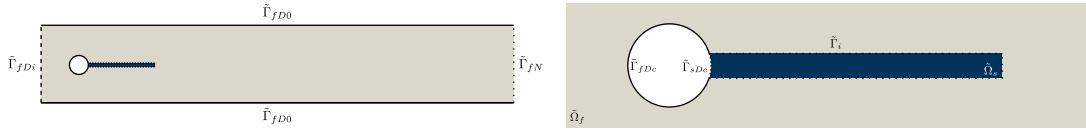
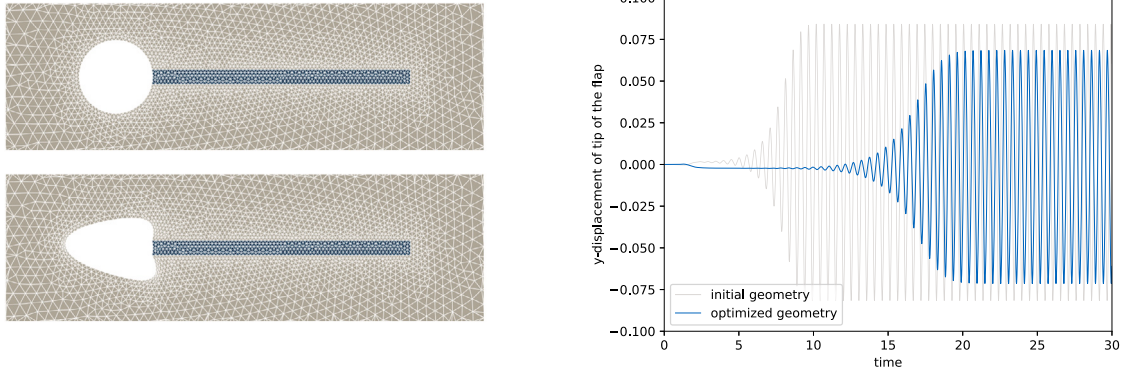
Fig. 2. Shape reference domain $\tilde{\Omega}$.

Fig. 3. Optimization of shape of obstacle (Section 6.1.1): Comparison of vertical displacement of the tip of the flap for the initial (top left) and optimized (bottom left) design.

Table 1

Optimization of shape of obstacle (Section 6.1.1): Optimization results when IPOPT converges up to an overall scaled NLP tolerance of 10^{-3} . The table shows the objective function value, the objective function value without the regularization and penalization term, the dual infeasibility and the number of linesearch-steps per iteration.

Iteration	Objective	Objective w/o reg. & pen.	Dual infeasibility	Linesearch-steps
0	1.5985e+02	1.5985e+02	2.27e+01	0
1	1.1851e+02	1.1569e+02	9.62e+00	2
2	1.1436e+02	1.1060e+02	4.40e+00	1
3	1.1302e+02	1.0971e+02	2.43e+00	1
4	1.1162e+02	1.0818e+02	1.21e+01	3
5	1.0773e+02	1.0393e+02	5.75e+00	1
6	1.0756e+02	1.0349e+02	5.06e+00	1
7	1.0751e+02	1.0337e+02	1.01e+00	1
8	1.0747e+02	1.0336e+02	3.29e-01	1
9	1.0743e+02	1.0330e+02	3.69e-01	1
10	1.0730e+02	1.0316e+02	6.93e-01	1
11	1.0726e+02	1.0331e+02	4.60e-01	1
12	1.0725e+02	1.0333e+02	8.01e-01	2
13	1.0725e+02	1.0332e+02	8.10e-01	2
14	1.0725e+02	1.0329e+02	4.33e-03	1

6.1.1. Optimization of shape of obstacle

For a first example, $\tilde{\Gamma}_d = \tilde{\Gamma}_{fDc}$ serves as design boundary, i.e., we optimize the shape of the circular obstacle and keep the solid domain fixed. We impose a barycenter and volume constraint. In addition, we use the regularization parameter $\alpha = 0.1$ and we choose $\beta = 0.01$ in Eq. (7) for the weighting $\tilde{\beta}$ of the Laplace–Beltrami operator in (6). As constraints, we require that the volume and barycenter of the obstacle remain the same as for the initial configuration. For our example, IPOPT converges after 14 iterations with an overall scaled NLP error (cf. [61, p. 3, (5)]) smaller than $1 \cdot 10^{-3}$, see Table 1. In this table, also other quantities of the optimizer’s output are shown, such as the dual infeasibility [61, (4a)] and the number of linesearch steps [61, Section 4.1]. The objective function value is reduced by more than 30 %. Fig. 3 compares the initial configuration and the optimized configuration. The vertical displacement of the tip of the flap shows that even though the optimization is only performed on the first 15 seconds the amplitude of the vertical displacement of the tip of the flap is also smaller for long-term simulations.

6.1.2. Optimization of interface

For a second example, we choose the interface $\tilde{\Gamma}_d = \tilde{\Gamma}_i$ as design boundary. Here, we use the regularization parameter $\alpha = 10$ and weighting for the Laplace–Beltrami operator $\beta = 10^{-3}$. Too small values for the regularization parameter α lead to poor convergence.

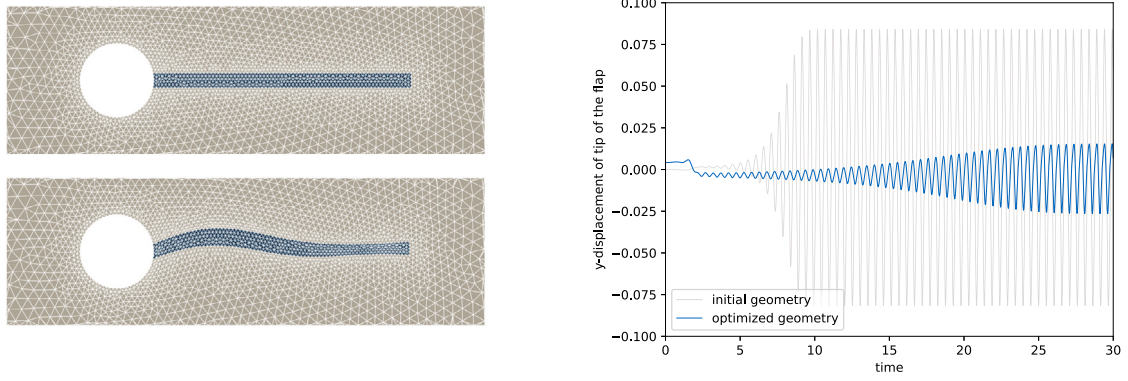


Fig. 4. Optimization of interface (Section 6.1.2): Comparison of vertical displacement of the tip of the flap for the initial (top left) and optimized (bottom left) design. The initial displacement of the tip of the flap for the optimized design is not plotted as zero, because the tip of the optimized flap is located at (0.597718, 0.20417) instead of (0.6, 0.2).

Table 2

Optimization of interface (Section 6.1.2): Optimization results when IPOPT converges up to an overall scaled NLP tolerance of 10^{-3} . The table shows the objective function value, the objective function value without the regularization and penalization term, the dual infeasibility and the number of linesearch-steps per iteration.

Iteration	Objective	Objective w/o reg. & pen.	Dual infeasibility	Linesearch-steps
0	1.5985e+02	1.5985e+02	3.85e+01	0
1	1.4593e+02	1.4479e+02	1.67e+01	10
2	1.3925e+02	1.3592e+02	1.46e+01	1
3	1.3246e+02	1.2996e+02	5.85e+00	1
4	1.2932e+02	1.2732e+02	2.91e+00	1
5	1.2782e+02	1.2612e+02	1.37e+00	1
6	1.2757e+02	1.2567e+02	3.63e-01	1
7	1.2754e+02	1.2565e+02	3.08e-01	1
8	1.2744e+02	1.2541e+02	2.26e-01	1
9	1.2743e+02	1.2528e+02	3.08e-02	1
10	1.2743e+02	1.2528e+02	1.99e-02	1
11	1.2743e+02	1.2528e+02	4.49e-03	1
12	1.2743e+02	1.2528e+02	5.56e-03	2
13	1.2743e+02	1.2528e+02	4.85e-03	1
14	1.2743e+02	1.2527e+02	9.04e-04	1

As constraint, we impose that the volume of the solid domain remains the same as for the initial configuration. For this example, IPOPT converges after 14 iterations with an overall scaled NLP error smaller than $1 \cdot 10^{-3}$, see Table 2. The objective function value is reduced by more than 20 %. As for the previous example, Fig. 4 compares the initial configuration and the optimized configuration.

6.2. Further numerical examples

We present further numerical test cases. As constraint, we impose that the volume of the elastic structure does not change compared to the initial configuration. If not explicitly stated differently, the choice of the parameters, initial and boundary conditions is the same as for the FSI2 benchmark.

6.2.1. Lift minimization I

Analogously to the FSI2 benchmark, we consider a two-dimensional rectangular domain of length $l = 2.5$ and height $h = 0.41$ with the parabolic inflow on the left boundary given by $\tilde{\mathbf{v}}_{fD}$. In this pipe there is a circular hole centered at $\mathbf{m} = (0.2, 0.2)$ with radius $r = 0.0125$, which is surrounded by an elastic structure. The elastic structure is drop-shaped with a tip at $\mathbf{p} = (0.3, 0.2)$ and drop radius $2r = 0.025$ around \mathbf{m} , as depicted in Fig. 6. Instead of optimizing the drag, we minimize the mean lift, which corresponds to replacing $\tilde{\boldsymbol{\psi}} = (1, 0)^T$ by $\tilde{\boldsymbol{\psi}} = (0, 1)^T$ in Section 3.2. We choose $T = 7.5$ s, $\alpha = 10$ and $\beta = 10^{-3}$. As before, we plot the vertical displacement of the tip of the elastic structure for a larger time horizon (for this example $T = 15$ s) and present the output of the optimization algorithm in Table 3.

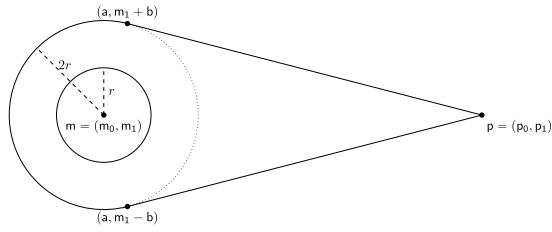


Fig. 5. Sketch of drop-shaped geometry considered in Section 6.2.1 where, for $p_1 = m_1$, $a = \frac{-m_0 p_0 + m_0^2 - (2r)^2}{(m_0 - p_0)}$ and $b = \sqrt{(2r)^2 - (a - m_0)^2}$.

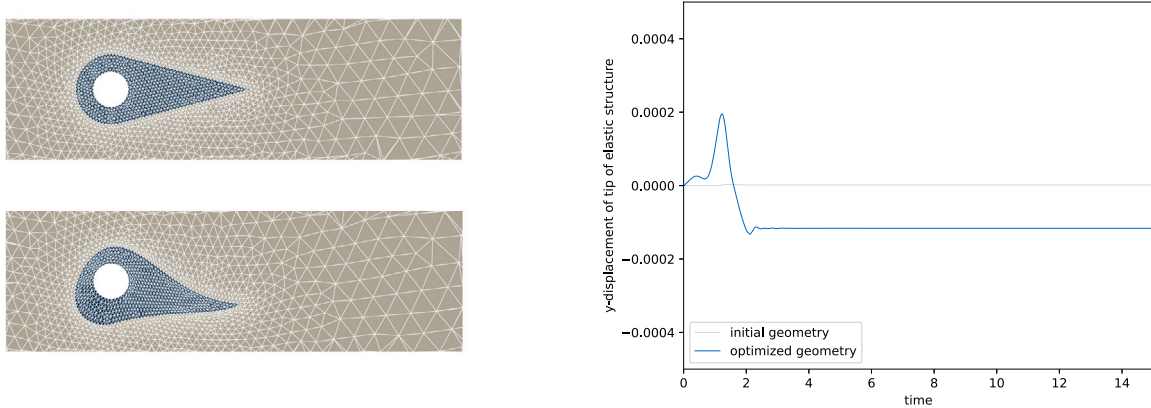


Fig. 6. Lift minimization (Section 6.2.1): Comparison of vertical displacement of the tip of the flap for the initial (top left) and optimized (bottom left) design. Here, different from Fig. 4 and due to the small displacements, the plot is not shifted for the optimized structure.

Table 3

Lift minimization (Section 6.2.1): Optimization results when IPOPT converges up to an overall NLP tolerance of 10^{-3} . The table shows the objective function value, the objective function value without the regularization and penalization term, the dual infeasibility and the number of linesearch-steps per iteration.

Iteration	Objective	Objective w/o reg. & pen.	Dual infeasibility	Linesearch-steps
0	$-6.3260e-02$	$-6.3901e-02$	$6.96e+00$	0
1	$-6.1103e+00$	$-6.5284e+00$	$4.12e+00$	8
2	$-7.8561e+00$	$-8.3784e+00$	$3.15e+00$	1
3	$-1.3871e+01$	$-2.7976e+01$	$4.64e+00$	1
4	$-1.4959e+01$	$-2.6364e+01$	$4.67e+00$	1
5	$-1.6050e+01$	$-2.4853e+01$	$2.60e-01$	1
6	$-1.6089e+01$	$-2.5736e+01$	$1.59e-01$	1
7	$-1.6102e+01$	$-2.5966e+01$	$6.90e-02$	1
8	$-1.6105e+01$	$-2.6059e+01$	$4.59e-03$	1

6.2.2. Lift minimization II

We further discuss our choice of $\tilde{\beta}$ (see (7)). We consider a drop-shaped obstacle, as depicted in Fig. 7 with $m = (0.2, 0.2)$, $p = (0.3, 0.2)$ and $2r = 0.025$. Similar to the geometrical setting introduced in Section 6.2.1, it is considered as an obstacle in a rectangular domain of length $l = 2.5$ and height $h = 0.41$. In this modified set-up, the interface, which serves as design boundary, consists of two lines and has a boundary itself. As in the previous section, we optimize the interface such that the lift of the obstacle is minimized. We present numerical results for minimizing the mean lift for $T = 7.5$ s for $\tilde{\beta}$ as proposed in (7) and for $\alpha = 0.1$ and $\beta = 10^{-3}$ (see Fig. 8 and Table 4).

Remark 4. Note that the optimal solutions depend on several choices such as, e.g., the parameterization of the set of admissible shapes via the boundary and extension operators, the choice of the regularization parameter and the threshold for the determinant constraint. For the presented results, these parameters have been chosen via some experimentation. While, e.g., for too large choices of α the regularization term has a strong influence, too small choices of α can impair the performance of the optimization algorithm. To circumvent these difficulties, the parameters can be chosen adaptively. Moreover, the presented method can be used as a building block of an outer iterative procedure, where the (potentially remeshed) optimized geometry of the previous step is used as initial

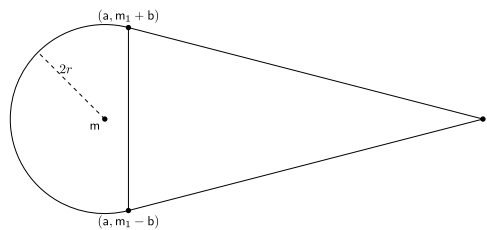


Fig. 7. Sketch of drop-shaped geometry considered in Section 6.2.2 with a and b as in Fig. 5.

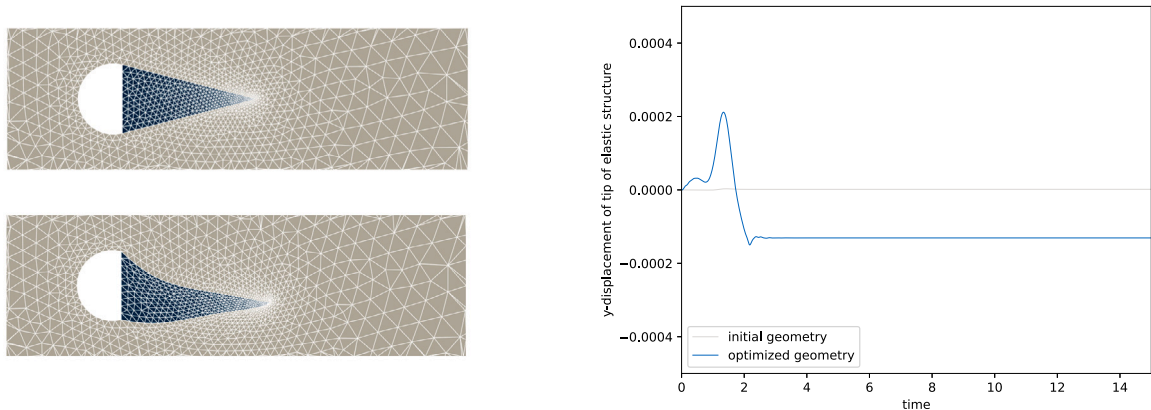


Fig. 8. Lift minimization (Section 6.2.2): Comparison of vertical displacement of the tip of the flap for the initial (top left) and optimized (bottom left) design. Here, as in Fig. 6, the plot is not shifted for the optimized structure.

Table 4

Lift minimization (Section 6.2.2): Optimization results when IPOPT converges up to an overall NLP tolerance of 10^{-3} . The table shows the objective function value, the objective function value without the regularization and penalization term, the dual infeasibility and the number of linesearch-steps per iteration.

Iteration	Objective	Objective w/o reg. & pen.	Dual infeasibility	Linesearch-steps
0	$-9.0850e-02$	$-9.1490e-02$	$7.22e+00$	0
1	$-5.4782e+00$	$-5.4955e+00$	$7.01e+00$	7
2	$-8.2569e+00$	$-8.2634e+00$	$1.24e+00$	1
3	$-8.2690e+00$	$-8.2762e+00$	$2.79e-01$	1
4	$-8.2912e+00$	$-8.2986e+00$	$3.35e-01$	1
5	$-9.1824e+00$	$-9.2328e+00$	$1.20e+00$	1
6	$-9.3000e+00$	$-9.3929e+00$	$8.79e-01$	2
7	$-9.4488e+00$	$-9.6434e+00$	$2.04e-01$	1
8	$-9.4816e+00$	$-9.6436e+00$	$6.54e-02$	1

domain for the next step and every outer iterate fulfills the constraints up to a certain, user-specified tolerance. This can lead to refined results, see, e.g., [26] for Stokes flow.

7. Conclusion and outlook

We applied the method of mappings to solve a shape optimization problem for unsteady FSI. We introduced the FSI model and show in the Appendix that the adjoint equations for a linearized version of the model attain the same structure as the forward equations. Performing shape optimization via the method of mappings requires the transformation of these equations to a reference domain. The choice of admissible shape transformations is done in a sophisticated manner in order to have a well-posed optimization problem. One of the main challenges is the prevention of mesh degeneration during the optimization process, which is done with a formulation of the optimization method respecting the continuous requirements for the transformations and adding a penalization of too small determinant values of the gradient of the transformation. As objective function a volume formulation of the drag of the obstacle is chosen. Numerical results show the viability of the approach to optimize the shape of the obstacle's boundary and of the interface based on problems derived from the FSI2 benchmark. There are several degrees of freedom in realizing the method of mappings, e.g., via the choice of the boundary operator and the extension operator. Moreover, also iterative approaches can be

considered, where the optimized shape serves as initial shape for the next iteration. This can also be combined with remeshing routines and parameter tuning. In addition, to make the algorithm more robust, the determinant constraint can also be imposed on an hold all domain that includes the obstacle.

CRediT authorship contribution statement

Johannes Haubner: Writing – original draft, Visualization, Software, Methodology, Formal analysis. **Michael Ulbrich:** Writing – review & editing, Supervision, Methodology, Funding acquisition, Formal analysis, Conceptualization.

Declaration of competing interest

The authors declare that they have no known competing financial interests or personal relationships that could have appeared to influence the work reported in this paper.

Data availability

Code is publicly available on URL <https://github.com/JohannesHaubner/ShapeOpt/>.

Acknowledgments

This work was funded by the Deutsche Forschungsgemeinschaft (DFG, German Research Foundation) as part of the International Research Training Group IGDK 1754 “Optimization and Numerical Analysis for Partial Differential Equations with Nonsmooth Structures” – Project Number 188264188/GRK1754, and the Research Council of Norway, grant 300305. Johannes Haubner would like to acknowledge Jørgen S. Dokken, Henrik N. Finsberg and Simon W. Funke for the support and discussions on reproducibility of numerical results. This article was published as Open Access with the financial support of the University of Graz.

Appendix. Adjoint for a linear unsteady FSI problem with stationary interface

For efficient derivative computations in optimal control, the adjoint equations have to be solved. Especially in cases where no automatic differentiation can be applied, it is crucial to derive an explicit formula for the adjoint equations. Even though the FSI model is modified for performing shape optimization, the adjoint equations to the unmodified model can be used to compute the derivative. This can be realized by performing every iteration on the current ALE reference domain instead of the nominal domain, cf. [17, Sec. 2.2.2]. In our choice of the software framework, automatic differentiation is available and the following considerations are not needed for the numerical implementation. Nevertheless, we think that the result might be of interest for some readers.

We consider the adjoint of a linear version of the fluid–structure interaction model (1). More precisely, we consider Stokes flow for the fluid and linear elasticity for the solid equations. Additionally, we restrict ourselves to the case with a stationary interface $\hat{\Gamma}_i$ and homogeneous Dirichlet boundary conditions, i.e., $\hat{\Omega} = \hat{\Omega}(t) = \Omega$ and $\partial\Omega(t) = \hat{\Gamma}_{fD} \cup \hat{\Gamma}_{sD}$ for any $t \in I$. This also implies that $\hat{\chi} = \text{id}_Y$, $\hat{J}_\chi = 1$ and $\hat{\mathbf{F}}_\chi = \mathbf{I}$. The resulting fluid–structure interaction problem (for better readability without subscripts for the state variables and without superscripts) reads as follows

$$\begin{aligned} \rho_f \partial_t \mathbf{v} - \text{div}(\sigma_f) &= \rho_f \mathbf{f}_f & \text{in } Q_f^T, \\ \text{div}(\mathbf{v}) &= 0 & \text{in } Q_f^T, \\ \rho_s \partial_t \mathbf{v} - \text{div}(\sigma_s) &= \rho_s \mathbf{f}_s & \text{in } Q_s^T, \\ \rho_s (\partial_t \mathbf{w} - \mathbf{v}) &= 0 & \text{in } Q_s^T, \end{aligned} \tag{A.1}$$

with the initial conditions

$$\mathbf{v}(\cdot, 0) = \mathbf{v}_0 \quad \text{on } \Omega_f, \quad \mathbf{w}(\cdot, 0) = \mathbf{w}_0 \quad \text{on } \Omega_s, \quad \mathbf{v}(\cdot, 0) = \mathbf{v}_0 \quad \text{on } \Omega_s,$$

boundary conditions

$$\mathbf{v} = 0 \quad \text{on } \Sigma_f^T, \quad \mathbf{w} = 0 \quad \text{on } \Sigma_s^T,$$

and the additional coupling conditions

$$\partial_t \mathbf{w} = \mathbf{v} \quad \text{on } \Sigma_i^T, \quad -\sigma_f \mathbf{n}_f = \sigma_s \mathbf{n}_s \quad \text{on } \Sigma_i^T,$$

where $\sigma_f = \mu_f (D\mathbf{v} + D\mathbf{v}^T) - p\mathbf{I}$, $\mu_f = \rho_f \nu_f$, $\sigma_s = \mu_s (D\mathbf{w} + D\mathbf{w}^T) + \lambda_s \text{div}(\mathbf{w})\mathbf{I}$ and, for the sake of convenience, we introduced \mathbf{v}_0 defined by $\mathbf{v}_0|_{\Omega_f} = \mathbf{v}_{0f}$ and $\mathbf{v}_0|_{\Omega_s} = \mathbf{w}_1$. For compatibility reasons there holds $\mathbf{w}_0|_{\Gamma_s} = 0$. This corresponds to the setting considered in [65].

We are interested in the structure of the adjoint equations and therefore do calculations on a formal level in order to derive a formulation for the adjoint system. In particular, we do not analyze the regularity of solutions but only assume that all functions are smooth enough such that the appearing terms and operations are well-defined. For the analysis of (A.1) we refer to [65–67]. As usual for unsteady problems, the flow of information in the adjoint equation is reversed in time. In order to transfer the theory and numerical methods from the forward model to the adjoint, it is desirable that, except for time reversal, the adjoint system has

a similar or the same structure as the forward model. In our approach the adjoint has the same structure as the FSI system (A.1). In [67], it is shown that a straightforward weak formulation can fail to have the desired property, basically due to the equation $\partial_t \mathbf{w} - \mathbf{v} = 0$. As a remedy, it is proposed in [67] to work with $\nabla \partial_t \mathbf{w} - \nabla \mathbf{v} = 0$ instead. In the following, we apply ideas from [65] to reformulate the weak formulation and obtain an analogous result.

We introduce $\mathbf{W}(\mathbf{v})(\cdot, t) = \mathbf{w}_0 + \int_0^t \mathbf{v}(\cdot, s) ds$. Since $\mathbf{w}(\cdot, 0) = \mathbf{w}_0$ and $\partial_t \mathbf{w} - \mathbf{v} = 0$ on Ω_s , we can substitute $\mathbf{w}(\cdot, t) = \mathbf{w}_0 + \int_0^t \mathbf{v}(\cdot, s) ds = \mathbf{W}(\mathbf{v})(\cdot, t)$ on Ω_s into (A.1). If \mathbf{w} is smooth enough such that the trace $\partial_t \mathbf{w}|_{\Sigma_s^T}$ exists, we obtain from $\partial_t \mathbf{w} - \mathbf{v} = 0$ on Q_s^T and $\mathbf{w}|_{\Sigma_s^T} = 0$ that $\mathbf{v}|_{\Sigma_s^T} = 0$. One can check that $\rho_s(\partial_t \mathbf{W}(\mathbf{v}) - \mathbf{v}) = 0$ on Q_s^T , $\mathbf{W}(\mathbf{v}) = 0$ on Σ_s^T , and $\mathbf{W}(\mathbf{v})(\cdot, 0) = \mathbf{w}_0$ are satisfied by the definition of $\mathbf{W}(\mathbf{v})$. Moreover, $\partial_t \mathbf{W}(\mathbf{v}) = \mathbf{v}$ on Σ_i^T is satisfied if we require $\mathbf{v}(\cdot, t) \in H_0^1(\Omega)$ for almost all $t \in I$, which implies uniqueness of the trace. Thus, system (A.1) with its initial, boundary and coupling conditions is equivalent to:

$$\begin{aligned} \rho_f \partial_t \mathbf{v} - \mu_f \operatorname{div}(D\mathbf{v} + D\mathbf{v}^T) + \nabla p &= \rho_f \mathbf{f}_f & \text{in } Q_f^T, \\ \operatorname{div}(\mathbf{v}) &= 0 & \text{in } Q_f^T, \\ \mathbf{v} &= 0 & \text{on } \Sigma_f^T, \\ \rho_s \partial_t \mathbf{v} - \mu_s \operatorname{div}(D(\mathbf{W}(\mathbf{v})) + D(\mathbf{W}(\mathbf{v}))^T) - \lambda_s \nabla(\operatorname{div}(\mathbf{W}(\mathbf{v}))) &= \rho_s \mathbf{f}_s & \text{in } Q_s^T, \\ \mathbf{v} &= 0 & \text{on } \Sigma_s^T, \\ \mathbf{v}(\cdot, 0) &= \mathbf{v}_0 & \text{on } \Omega, \end{aligned} \quad (\text{A.2})$$

with the additional coupling condition

$$p\mathbf{n}_f - \mu_f(D\mathbf{v} + D\mathbf{v}^T)\mathbf{n}_f = \mu_s(D(\mathbf{W}(\mathbf{v})) + D(\mathbf{W}(\mathbf{v}))^T)\mathbf{n}_s + \lambda_s \operatorname{div}(\mathbf{W}(\mathbf{v}))\mathbf{n}_s \text{ on } \Sigma_i^T.$$

The following notation is used:

- $(p, q)_\Omega := \int_\Omega p q d\xi$ for all $p, q \in L^2(\Omega)$, $(\mathbf{v}, \mathbf{u})_\Omega := \int_\Omega \mathbf{v} \cdot \mathbf{u} d\xi$ for all $\mathbf{v}, \mathbf{u} \in L^2(\Omega)^d$ and $(\mathbf{A}, \mathbf{B})_\Omega := \int_\Omega \mathbf{A} : \mathbf{B} d\xi$ for all $\mathbf{A}, \mathbf{B} \in L^2(\Omega)^{d \times d}$.
- $(\mathbf{v}, \mathbf{u})_\Gamma := \int_\Gamma \mathbf{v} \cdot \mathbf{u} dS(\xi)$ for all $\mathbf{v}, \mathbf{u} \in L^2(\Gamma)^d$, where $dS(\xi)$ is the surface measure on Γ .
- $\langle\langle p, q \rangle\rangle_{Q^T} := \int_0^T (p(\cdot, t), q(\cdot, t))_\Omega dt$ for all $p, q \in L^2((0, T), L^2(\Omega))$,
 $\langle\langle \mathbf{v}, \mathbf{u} \rangle\rangle_{Q^T} := \int_0^T (\mathbf{v}(\cdot, t), \mathbf{u}(\cdot, t))_\Omega dt$ for all $\mathbf{v}, \mathbf{u} \in L^2((0, T), L^2(\Omega)^d)$ and
 $\langle\langle \mathbf{A}, \mathbf{B} \rangle\rangle_{Q^T} := \int_0^T (\mathbf{A}, \mathbf{B})_\Omega dt$ for all $\mathbf{A}, \mathbf{B} \in L^2((0, T), L^2(\Omega)^{d \times d})$.
- $a_f(\mathbf{v}, \mathbf{z}) = \frac{\mu_f}{2} (D\mathbf{v} + D\mathbf{v}^T, D\mathbf{z} + D\mathbf{z}^T)_{\Omega_f}$,
 $a_s(\mathbf{v}, \mathbf{z}) = \frac{\mu_s}{2} (D\mathbf{v} + D\mathbf{v}^T, D\mathbf{z} + D\mathbf{z}^T)_{\Omega_s} + \lambda_s (\operatorname{div}(\mathbf{v}), \operatorname{div}(\mathbf{z}))_{\Omega_s}$, for $\mathbf{v}, \mathbf{z} \in H_0^1(\Omega)^d$.

For vector valued variables \mathbf{v} and \mathbf{z} , we use the identities

$$\begin{aligned} (\mathbf{A}, D\mathbf{z})_\Omega &= -(\operatorname{div}(\mathbf{A}), \mathbf{z})_\Omega + (\mathbf{A}\mathbf{n}, \mathbf{z})_{\partial\Omega}, \\ (\operatorname{div}(\mathbf{v}), \operatorname{div}(\mathbf{z}))_\Omega &= -(\nabla \operatorname{div}(\mathbf{v}), \mathbf{z})_\Omega + (\operatorname{div}(\mathbf{v})\mathbf{n}, \mathbf{z})_{\partial\Omega}. \end{aligned} \quad (\text{A.3})$$

Testing (A.2) with (ψ^v, ψ^p) such that $\psi^v|_{\partial\Omega \times I} = 0$ gives:

$$\begin{aligned} &\rho_f \langle\langle \partial_t \mathbf{v}, \psi^v \rangle\rangle_{Q_f^T} - \mu_f \langle\langle \operatorname{div}(D\mathbf{v} + D\mathbf{v}^T), \psi^v \rangle\rangle_{Q_f^T} \\ &+ \langle\langle \nabla p, \psi^v \rangle\rangle_{Q_f^T} - \langle\langle \rho_f \mathbf{f}_f, \psi^v \rangle\rangle_{Q_f^T} + \rho_s \langle\langle \partial_t \mathbf{v}, \psi^v \rangle\rangle_{Q_s^T} \\ &- \langle\langle \rho_s \mathbf{f}_s, \psi^v \rangle\rangle_{Q_s^T} - \langle\langle \operatorname{div}(\mathbf{v}), \psi^p \rangle\rangle_{Q_f^T} \\ &+ \rho_f (\mathbf{v}(\cdot, 0) - \mathbf{v}_0, \psi^v(\cdot, 0))_{\Omega_f} + \rho_s (\mathbf{v}(\cdot, 0) - \mathbf{v}_0, \psi^v(\cdot, 0))_{\Omega_s} \\ &- \mu_s \langle\langle \operatorname{div}(D(\mathbf{W}(\mathbf{v})) + D(\mathbf{W}(\mathbf{v}))^T), \psi^v \rangle\rangle_{Q_s^T} - \lambda_s \langle\langle \nabla(\operatorname{div}(\mathbf{W}(\mathbf{v}))), \psi^v \rangle\rangle_{Q_s^T} = 0. \end{aligned} \quad (\text{A.4})$$

With (A.3), $\mathbf{v}|_{\partial\Omega \times I} = 0$, and the identity $(\mathbf{A}^T, \mathbf{B}^T)_\Omega = (\mathbf{A}, \mathbf{B})_\Omega$ we obtain the formulas

$$\begin{aligned} \mu_f \langle\langle \operatorname{div}(D\mathbf{v} + D\mathbf{v}^T), \psi^v \rangle\rangle_{\Omega_f} &= -a_f(\mathbf{v}, \psi^v) + \mu_f ((D\mathbf{v} + D\mathbf{v}^T)\mathbf{n}_f, \psi^v)_{\Gamma_i}, \\ (\nabla p, \psi^v)_{\Omega_f} &= -(p, \operatorname{div}(\psi^v))_{\Omega_f} + (p\mathbf{n}_f, \psi^v)_{\partial\Omega_f} = -(p, \operatorname{div}(\psi^v))_{\Omega_f} + (p\mathbf{n}_f, \psi^v)_{\Gamma_i}, \end{aligned}$$

and

$$\begin{aligned} &\mu_s \langle\langle \operatorname{div}(D\mathbf{w} + D\mathbf{w}^T), \psi^v \rangle\rangle_{\Omega_s} + \lambda_s \langle\langle \nabla(\operatorname{div}(\mathbf{w})), \psi^v \rangle\rangle_{\Omega_s} \\ &= -\frac{\mu_s}{2} (D\mathbf{w} + D\mathbf{w}^T, D\psi^v + D\psi^{v^T})_{\Omega_s} + \mu_s ((D\mathbf{w} + D\mathbf{w}^T)\mathbf{n}_s, \psi^v)_{\Gamma_i} \\ &\quad - \lambda_s (\operatorname{div}(\mathbf{w}), \operatorname{div}(\psi^v))_{\Omega_s} + \lambda_s (\operatorname{div}(\mathbf{w})\mathbf{n}_s, \psi^v)_{\Gamma_i} \\ &= -a_s(\mathbf{w}, \psi^v) + \mu_s ((D\mathbf{w} + D\mathbf{w}^T)\mathbf{n}_s, \psi^v)_{\Gamma_i} + \lambda_s (\operatorname{div}(\mathbf{w})\mathbf{n}_s, \psi^v)_{\Gamma_i}. \end{aligned}$$

Thus, (A.4) can be reformulated as

$$\rho_f \langle\langle \partial_t \mathbf{v}, \psi^v \rangle\rangle_{Q_f^T} + \int_0^T a_f(\mathbf{v}, \psi^v) dt - \langle\langle p, \operatorname{div}(\psi^v) \rangle\rangle_{Q_f^T}$$

$$\begin{aligned}
& + \rho_s \langle \partial_t \mathbf{v}, \boldsymbol{\psi}^v \rangle_{Q_s^T} + \int_0^T a_s(\mathbf{W}(\mathbf{v}), \boldsymbol{\psi}^v) dt - \langle \text{div}(\mathbf{v}), \boldsymbol{\psi}^p \rangle_{Q_f^T} \\
& - \langle \rho_f \mathbf{f}_f, \boldsymbol{\psi}^v \rangle_{Q_f^T} - \langle \rho_s \mathbf{f}_s, \boldsymbol{\psi}^v \rangle_{Q_s^T} \\
& + \rho_f \langle \mathbf{v}(\cdot, 0) - \mathbf{v}_0, \boldsymbol{\psi}^v(\cdot, 0) \rangle_{\Omega_f} + \rho_s \langle \mathbf{v}(\cdot, 0) - \mathbf{v}_0, \boldsymbol{\psi}^v(\cdot, 0) \rangle_{\Omega_s} \\
& - \int_0^T (\mu_f(D\mathbf{v} + D\mathbf{v}^\top) \mathbf{n}_f - p \mathbf{n}_f + \mu_s(D\mathbf{W}(\mathbf{v}) + D\mathbf{W}(\mathbf{v})^\top) \mathbf{n}_s \\
& \quad + \lambda_s \text{div}(\mathbf{W}(\mathbf{v})) \mathbf{n}_s, \boldsymbol{\psi}^v)_{\Gamma_1} dt = 0,
\end{aligned}$$

which, by inserting the interface condition, yields the weak formulation

$$\begin{aligned}
& \rho_f \langle \partial_t \mathbf{v}, \boldsymbol{\psi}^v \rangle_{Q_f^T} + \int_0^T a_f(\mathbf{v}, \boldsymbol{\psi}^v) dt - \langle p, \text{div}(\boldsymbol{\psi}^v) \rangle_{Q_f^T} \\
& + \rho_s \langle \partial_t \mathbf{v}, \boldsymbol{\psi}^v \rangle_{Q_s^T} + \int_0^T a_s(\mathbf{W}(\mathbf{v}), \boldsymbol{\psi}^v) dt - \langle \text{div}(\mathbf{v}), \boldsymbol{\psi}^p \rangle_{Q_f^T} \\
& - \langle \rho_f \mathbf{f}_f, \boldsymbol{\psi}^v \rangle_{Q_f^T} - \langle \rho_s \mathbf{f}_s, \boldsymbol{\psi}^v \rangle_{Q_s^T} \\
& + \rho_f \langle \mathbf{v}(\cdot, 0) - \mathbf{v}_0, \boldsymbol{\psi}^v(\cdot, 0) \rangle_{\Omega_f} + \rho_s \langle \mathbf{v}(\cdot, 0) - \mathbf{v}_0, \boldsymbol{\psi}^v(\cdot, 0) \rangle_{\Omega_s} = 0.
\end{aligned}$$

Hence, the linear PDE can be written as $\langle A(\boldsymbol{\eta}^v, \boldsymbol{\eta}^p), (\boldsymbol{\psi}^v, \boldsymbol{\psi}^p) \rangle = \langle F, \boldsymbol{\psi}^v \rangle$, where the operator A is defined by

$$\begin{aligned}
\langle A(\boldsymbol{\eta}^v, \boldsymbol{\eta}^p), (\boldsymbol{\psi}^v, \boldsymbol{\psi}^p) \rangle & = \rho_f \langle \partial_t \boldsymbol{\eta}^v, \boldsymbol{\psi}^v \rangle_{Q_f^T} + \int_0^T a_f(\boldsymbol{\eta}^v, \boldsymbol{\psi}^v) dt - \langle \boldsymbol{\eta}^p, \text{div}(\boldsymbol{\psi}^v) \rangle_{Q_f^T} \\
& + \rho_s \langle \partial_t \boldsymbol{\eta}^v, \boldsymbol{\psi}^v \rangle_{Q_s^T} + \int_0^T a_s \left(\int_0^t \boldsymbol{\eta}^v(\cdot, s) ds, \boldsymbol{\psi}^v \right) dt - \langle \text{div}(\boldsymbol{\eta}^v), \boldsymbol{\psi}^p \rangle_{Q_f^T} \\
& + \rho_f \langle \boldsymbol{\eta}^v(\cdot, 0), \boldsymbol{\psi}^v(\cdot, 0) \rangle_{\Omega_f} + \rho_s \langle \boldsymbol{\eta}^v(\cdot, 0), \boldsymbol{\psi}^v(\cdot, 0) \rangle_{\Omega_s}.
\end{aligned}$$

We are interested in the operator A^* . The term which destroys the symmetry of the operator A is given by a_s . A closer consideration of this term yields (under the assumption that we are on spaces where Fubini's theorem is valid):

$$\begin{aligned}
& \int_0^T a_s \left(\int_0^t \boldsymbol{\eta}^v(\cdot, s) ds, \boldsymbol{\psi}^v \right) dt = \int_0^T a_s \left(\int_0^t \boldsymbol{\eta}^v(\cdot, s) ds, \boldsymbol{\psi}^v(\cdot, t) \right) dt \\
& = \int_0^T \int_0^t a_s(\boldsymbol{\eta}^v(\cdot, s), \boldsymbol{\psi}^v(\cdot, t)) ds dt = \int_0^T \int_s^T a_s(\boldsymbol{\eta}^v(\cdot, s), \boldsymbol{\psi}^v(\cdot, t)) dt ds \\
& = \int_0^T a_s(\boldsymbol{\eta}^v(\cdot, s), \int_s^T \boldsymbol{\psi}^v(\cdot, t) dt) ds = \int_0^T a_s(\boldsymbol{\eta}^v(\cdot, s), \int_0^{T-s} \boldsymbol{\psi}^v(\cdot, T-t) dt) ds \\
& = \int_0^T a_s(\boldsymbol{\eta}^v(\cdot, T-s), \int_0^s \boldsymbol{\psi}^v(\cdot, T-t) dt) ds
\end{aligned}$$

Introducing $\bar{\boldsymbol{\eta}}^v(\xi, t) = \boldsymbol{\eta}^v(\xi, T-t)$, $\bar{\boldsymbol{\eta}}^p(\xi, t) = \boldsymbol{\eta}^p(\xi, T-t)$, $\bar{\boldsymbol{\psi}}^v(\xi, t) = \boldsymbol{\psi}^v(\xi, T-t)$, $\bar{\boldsymbol{\psi}}^p(\xi, t) = \boldsymbol{\psi}^p(\xi, T-t)$ yields

$$\int_0^T a_s \left(\int_0^t \boldsymbol{\eta}^v(\cdot, s) ds, \boldsymbol{\psi}^v \right) dt = \int_0^T a_s \left(\int_0^t \bar{\boldsymbol{\eta}}^v(\cdot, s) ds, \bar{\boldsymbol{\eta}}^v \right) dt.$$

We have $\partial_t \boldsymbol{\psi}^v(\cdot, t) = -\partial_s \bar{\boldsymbol{\psi}}^v(\cdot, s)$ for $s = T-t$ and the following equation holds true:

$$\begin{aligned}
\langle \boldsymbol{\eta}^v, \partial_t \boldsymbol{\psi}^v \rangle_{Q_f^T} & = \int_0^T \langle \boldsymbol{\eta}^v(\cdot, t), \partial_t \boldsymbol{\psi}^v(\cdot, t) \rangle_{\Omega_f} dt \\
& = \int_0^T \langle \bar{\boldsymbol{\eta}}^v(\cdot, T-t), -\partial_s \bar{\boldsymbol{\psi}}^v(\cdot, s)|_{s=T-t} \rangle_{\Omega_f} dt = - \int_0^T \langle \bar{\boldsymbol{\eta}}^v(\cdot, s), \partial_s \bar{\boldsymbol{\psi}}^v(\cdot, s) \rangle_{\Omega_f} ds \\
& = - \int_0^T \langle \bar{\boldsymbol{\eta}}^v(\cdot, t), \partial_t \bar{\boldsymbol{\psi}}^v(\cdot, t) \rangle_{\Omega_f} dt = - \langle \bar{\boldsymbol{\eta}}^v, \partial_t \bar{\boldsymbol{\psi}}^v \rangle_{Q_f^T}.
\end{aligned}$$

Thus, integration by parts yields

$$\begin{aligned}
\langle \partial_t \boldsymbol{\eta}^v, \boldsymbol{\psi}^v \rangle_{Q_f^T} & = [\langle \boldsymbol{\eta}^v(\cdot, t), \boldsymbol{\psi}^v(\cdot, t) \rangle_{\Omega_f}]_{t=0}^{t=T} - \langle \boldsymbol{\eta}^v, \partial_t \boldsymbol{\psi}^v \rangle_{Q_f^T} \\
& = \langle \boldsymbol{\eta}^v(\cdot, T), \boldsymbol{\psi}^v(\cdot, T) \rangle_{\Omega_f} - \langle \boldsymbol{\eta}^v(\cdot, 0), \boldsymbol{\psi}^v(\cdot, 0) \rangle_{\Omega_f} + \langle \bar{\boldsymbol{\eta}}^v, \partial_t \bar{\boldsymbol{\psi}}^v \rangle_{Q_f^T}, \\
\langle \partial_t \boldsymbol{\eta}^v, \boldsymbol{\psi}^v \rangle_{Q_s^T} & = \langle \boldsymbol{\eta}^v(\cdot, T), \boldsymbol{\psi}^v(\cdot, T) \rangle_{\Omega_s} - \langle \boldsymbol{\eta}^v(\cdot, 0), \boldsymbol{\psi}^v(\cdot, 0) \rangle_{\Omega_s} + \langle \bar{\boldsymbol{\eta}}^v, \partial_t \bar{\boldsymbol{\psi}}^v \rangle_{Q_s^T}.
\end{aligned}$$

Combining these results, rewriting the terms in $\bar{\boldsymbol{\eta}}^v$, $\bar{\boldsymbol{\eta}}^p$, $\bar{\boldsymbol{\psi}}^v$, $\bar{\boldsymbol{\psi}}^p$ and using that $(\boldsymbol{\eta}^v(\cdot, T), \boldsymbol{\psi}^v(\cdot, T))_{\Omega} = (\bar{\boldsymbol{\eta}}^v(\cdot, 0), \bar{\boldsymbol{\psi}}^v(\cdot, 0))_{\Omega}$ yields:

$$\begin{aligned}
\langle A(\boldsymbol{\eta}^v, \boldsymbol{\eta}^p), (\boldsymbol{\psi}^v, \boldsymbol{\psi}^p) \rangle & = \rho_f \langle \partial_t \bar{\boldsymbol{\psi}}^v, \bar{\boldsymbol{\eta}}^v \rangle_{Q_f^T} + \int_0^T a_f(\bar{\boldsymbol{\psi}}^v, \bar{\boldsymbol{\eta}}^v) dt - \langle \text{div}(\bar{\boldsymbol{\psi}}^v), \bar{\boldsymbol{\eta}}^p \rangle_{Q_f^T} \\
& + \rho_s \langle \partial_t \bar{\boldsymbol{\psi}}^v, \bar{\boldsymbol{\eta}}^v \rangle_{Q_s^T} + \int_0^T a_s \left(\int_0^t \bar{\boldsymbol{\psi}}^v(\cdot, s) ds, \bar{\boldsymbol{\eta}}^v \right) dt - \langle \bar{\boldsymbol{\psi}}^p, \text{div}(\bar{\boldsymbol{\eta}}^v) \rangle_{Q_f^T}
\end{aligned}$$

$$+ \rho_f(\bar{\psi}^v(\cdot, 0), \bar{\eta}^v(\cdot, 0))_{\Omega_f} + \rho_s(\bar{\psi}^v(\cdot, 0), \bar{\eta}^v(\cdot, 0))_{\Omega_s} = \langle A(\bar{\psi}^v, \bar{\psi}^p), (\bar{\eta}^v, \bar{\eta}^p) \rangle.$$

Thus, the adjoint has the same structure as the forward model, but reverses the temporal flow of information.

References

- [1] E. Dowell, K. Hall, Modeling of fluid-structure interaction, *Annu. Rev. Fluid Mech.* 33 (2001) 445–490.
- [2] J. Haubner, M. Ulbrich, S. Ulbrich, Analysis of shape optimization problems for unsteady fluid-structure interaction, *Inverse Problems* 36 (3) (2020) 38, <http://dx.doi.org/10.1088/1361-6420/ab5a11>, Id/No 034001.
- [3] C. Heinrich, R. Duvinneau, L. Blancard, Isogeometric Shape Optimization in Fluid-Structure Interaction, Research Report - RR7639, INRIA, 2011.
- [4] J. Heners, L. Radtke, M. Hinze, A. Düster, Adjoint shape optimization for fluid-structure interaction of ducted flows, *Comput. Mech.* 61 (3) (2017) 259–276.
- [5] M. Højat, E. Stavropoulou, T. Gallinger, U. Israel, R. Wüchner, K.-U. Bletzinger, Fluid-structure interaction in the context of shape optimization and computational wind engineering, in: H.-J. Bungartz, et al. (Eds.), *Fluid Structure Interaction II*, in: *Lecture Notes in Computational Science and Engineering*, vol. 73, Springer-Verlag, Berlin, Heidelberg, 2010, pp. 351–381.
- [6] M. Lombardi, N. Parolini, A. Quarteroni, G. Rozza, Numerical simulation of sailing boats: dynamics, FSI, and shape optimization, in: *Variational Analysis and Aerospace Engineering: Mathematical Challenges for Aerospace Design*, in: *Springer Optimization and Its Applications*, vol. 66, Springer-Verlag, New York, 2012, pp. 339–377.
- [7] C. Long, A. Marsden, Y. Bazilevs, Shape optimization of pulsatile ventricular assist devices using FSI to minimize thrombotic risk, *Comput. Mech.* 54 (4) (2014) 921–932.
- [8] M. Lund, H. Möller, L. Jakobsen, Shape design optimization of stationary fluid-structure interaction problems with large displacements and turbulence, *Struct. Multidiscip. Optim.* 25 (5) (2003) 383–392.
- [9] J. Martins, J. Alonso, J. Reuther, A coupled-adjoint sensitivity analysis method for high-fidelity aero-structural design, *Optim. Eng.* 6 (1) (2005) 33–62.
- [10] J. Martins, A. Lambe, Multidisciplinary design optimization: a survey of architectures, *AIAA J.* 51 (9) (2013) 2049–2075.
- [11] S. Shayegan, R. Najian Asl, A. Ghashtala, R. Wüchner, K.-U. Bletzinger, High Fidelity Aeroelastic Shape Optimization of Wind Turbine Blades using Vertex Morphing Method, in: *VII International Conference on Coupled Problems in Science and Engineering, ECCOMAS*, 2017.
- [12] H. Garcke, C. Hecht, M. Hinze, C. Kahle, K. Lam, Shape optimization for surface functionals in Navier-Stokes flow using a phase field approach, *Interfaces Free Bound.* 18 (2016) 137–159.
- [13] J. Haubner, F. Neumann, M. Ulbrich, A novel density based approach for topology optimization of Stokes flow, *SIAM J. Scient. Comput.* 45 (2) (2023) A338–A368, <http://dx.doi.org/10.1137/21m143114x>.
- [14] M.C. Delfour, J.-P. Zolésio, *Shapes and Geometries: Metrics, Analysis, Differential Calculus, and Optimization*, SIAM, Philadelphia, 2011.
- [15] F. Murat, J. Simon, Etude de problèmes d'optimal design, in: J. Cea (Ed.), *Optimization Techniques Modeling and Optimization in the Service of Man Part 2: Proceedings, 7th IFIP Conference Nice, September 8–12, 1975*, Springer-Verlag, Berlin, Heidelberg, 1976, pp. 54–62.
- [16] J. Bello, E. Fernández-Cara, J. Lemoine, J. Simon, The differentiability of the drag with respect to the variations of a Lipschitz domain in a Navier-Stokes flow, *SIAM J. Control Optim.* 35 (2) (1997) 626–640.
- [17] C. Brandenburg, F. Lindemann, M. Ulbrich, S. Ulbrich, A continuous adjoint approach to shape optimization for Navier Stokes flow, in: K. Kunisch, G. Leugering, J. Sprekels, F. Tröltzsch (Eds.), *Optimal Control of Coupled Systems of Partial Differential Equations*, in: *Internat. Ser. Numer. Math.*, vol. 160, Birkhäuser, Basel, 2009, pp. 35–56.
- [18] P. Guillaume, M. Masmoudi, Computation of high order derivatives in optimal shape design, *Numer. Math.* 67 (2) (1994) 231–250.
- [19] M. Keuthen, M. Ulbrich, Moreau–Yosida regularization in shape optimization with geometric constraints, *Comput. Optim. Appl.* 62 (1) (2015) 181–216.
- [20] M. Fischer, F. Lindemann, M. Ulbrich, S. Ulbrich, Fréchet differentiability of unsteady incompressible Navier–Stokes flow with respect to domain variations of low regularity by using a general analytical framework, *SIAM J. Control Optim.* 55 (5) (2017) 3226–3257.
- [21] A. Logg, K.-A. Mardal, G. Wells, *Automated Solution of Differential Equations by the Finite Element Method*, Springer-Verlag, Berlin, Heidelberg, 2012.
- [22] L. Radtke, G. Bletsos, N. Kühl, T. Suchan, T. Rung, A. Düster, K. Welker, Parameter-free shape optimization: various shape updates for engineering applications, *Aerospace* 10 (9) (2023) 751.
- [23] K. Deckelnick, P.J. Herbert, M. Hinze, A novel $W^{1,\infty}$ approach to shape optimisation with Lipschitz domains, *ESAIM Control Optim. Calc. Var.* 28 (2022) 2.
- [24] V.H. Schulz, M. Siebenborn, K. Welker, Efficient PDE constrained shape optimization based on Steklov–Poincaré-type metrics, *SIAM J. Optim.* 26 (4) (2016) 2800–2819.
- [25] J. Haubner, *Shape Optimization for Fluid-Structure Interaction* (Ph.D. thesis), Technische Universität München, München, 2020.
- [26] J. Haubner, M. Siebenborn, M. Ulbrich, A continuous perspective on shape optimization via domain transformations, *SIAM J. Scient. Comput.* 43 (3) (2021) A1997–A2018, <http://dx.doi.org/10.1137/20m1332050>.
- [27] J.S. Dokken, S.W. Funke, A. Johansson, S. Schmidt, Shape optimization using the finite element method on multiple meshes with Nitsche coupling, *SIAM J. Sci. Comput.* 41 (3) (2019) A1923–A1948.
- [28] J. Degroote, K. Bathe, J. Vierendeels, Performance of a new partitioned procedure versus a monolithic procedure in fluid-structure interaction, *Comput. Struct.* 87 (11–12) (2009) 793–801.
- [29] C. Kassiotis, A. Ibrahimbegovic, R. Niekamp, H. Matthies, Nonlinear fluid-structure interaction problem. Part I: implicit partitioned algorithm, nonlinear stability proof and validation examples, *Comput. Mech.* 47 (3) (2011) 305–323.
- [30] J. Donea, A. Huerta, J.-P. Ponthot, A. Rodríguez-Ferran, Arbitrary Lagrangian-Eulerian methods, in: *Encyclopedia of Computational Mechanics*, John Wiley & Sons, Ltd, Chichester, 2004, pp. 413–437.
- [31] T. Dunne, R. Rannacher, T. Richter, Numerical simulation of fluid-structure interaction based on monolithic variational formulations, in: *Fundamental Trends in Fluid-Structure Interaction*, in: *Contemporary Challenges in Mathematical Fluid Dynamics and Its Applications*, vol. 1, World Scientific Publishing Co. Pte. Ltd, Hackensack, NJ, 2010, pp. 1–75.
- [32] S. Frei, T. Richter, T. Wick, Eulerian techniques for fluid-structure interactions: Part I - Modeling and simulation, in: *Numerical Mathematics and Advanced Applications - ENUMATH 2013*, Springer International Publishing, Switzerland, 2015, pp. 745–753.
- [33] O. Ghattas, X. Li, A variational finite element method for stationary nonlinear fluid-solid interaction, *J. Comput. Phys.* 121 (2) (1995) 231–250.
- [34] A. Heil, A. Hazel, J. Boyle, Solvers for large-displacement fluid-structure interaction problems: segregated versus monolithic approaches, *Comput. Mech.* 43 (2008) 91–101.
- [35] T. Wick, Fully Eulerian fluid-structure interaction for time-dependent problems, *Comput. Methods Appl. Mech. Engrg.* 255 (2013) 14–26.
- [36] D. Coutand, S. Shkoller, Motion of an elastic solid inside an incompressible viscous fluid, *Arch. Ration. Mech. Anal.* 176 (1) (2005) 25–102.
- [37] M. Ignatova, I. Kukavica, I. Lasiecka, A. Tuffaha, Small data global existence for a fluid-structure model, *Nonlinearity* 30 (2) (2017) 848–898.
- [38] I. Kukavica, A. Tuffaha, Solutions to a fluid-structure interaction free boundary problem, *Discrete Contin. Dyn. Syst.* 32 (4) (2012) 1355–1389.
- [39] J.P. Raymond, M. Vanninathan, A fluid-structure model coupling the Navier-Stokes equations and the Lamé system, *J. Math. Pures Appl.* 102 (3) (2014) 546–596.
- [40] T. Wick, Fluid-structure interaction using different mesh motion techniques, *Comput. Struct.* (2011).

- [41] I. Harari, E. Grosu, A unified approach for embedded boundary conditions for fourth-order elliptic problems, *Internat. J. Numer. Methods Engrg.* 104 (7) (2015) 655–675.
- [42] B.T. Helenbrook, Mesh deformation using the biharmonic operator, *Internat. J. Numer. Methods Engrg.* 56 (7) (2003) 1007–1021.
- [43] V. John, G. Matthies, Higher-order finite element discretizations in a benchmark problem for incompressible flow, *Internat. J. Numer. Methods Fluids* 37 (2001) 885–903.
- [44] M. Braak, T. Richter, Solutions of 3D Navier-Stokes benchmark problems with adaptive finite elements, *Comput. & Fluids* 35 (4) (2006) 372–392.
- [45] J. Hoffman, C. Johnson, Adaptive finite element methods for incompressible fluid flow, in: *Error Estimation and Solution Adaptive Discretization in CFD: Lector Notes in Computational Science and Engineering*, Springer-Verlag, Berlin, Heidelberg, 2002, p. 122.
- [46] T. Edling, R. Herzog, E. Loayza, G. Wachsmuth, First and second order shape optimization based on restricted mesh deformations, *SIAM J. Sci. Comput.* 42 (2) (2020) A1200–A1225.
- [47] P. Michor, D. Mumford, Riemannian geometries on spaces of plane curves, *J. Eur. Math. Soc.* 8 (1) (2003) 1–48.
- [48] W. Ring, B. Wirth, Optimization methods on Riemannian manifolds and their application to shape space, *SIAM J. Optim.* 22 (2) (2012) 596–627.
- [49] H. Azegami, M. Shimoda, E. Katamine, Z.C. Wu, A domain optimization technique for elliptic boundary value problems, *WIT Trans. Built Environ.* 14 (1970).
- [50] T. Richter, T. Wick, On time discretizations of fluid-structure interactions, in: T. Carraro, M. Geiger, S. Körkel, R. Rannacher (Eds.), *Multiple Shooting and Time Domain Decomposition Methods*, Springer International Publishing, Switzerland, 2015, pp. 377–400.
- [51] T. Wick, Stability estimates and numerical comparison of second order time-stepping schemes for fluid-structure interactions, in: A. Cangiani, R. Davidchack, E. Georgoulis, A. Gorbunov, J. Levesley, M. Tretyakov (Eds.), *Numerical Mathematics and Advanced Applications 2011*, Springer-Verlag, Berlin, Heidelberg, 2013, pp. 625–632.
- [52] J.A. Iglesias, K. Sturm, F. Wechsung, Two-dimensional shape optimization with nearly conformal transformations, *SIAM J. Sci. Comput.* 40 (6) (2018) A3807–A3830.
- [53] S. Basting, A. Quaini, S. Čanić, R. Glowinski, Extended ALE method for fluid–structure interaction problems with large structural displacements, *J. Comput. Phys.* 331 (2017) 312–336.
- [54] C. Elliott, H. Fritz, On algorithms with good mesh properties for problems with moving boundaries based on the Harmonic Map Heat Flow and the DeTurck trick, *SMAI J. Comput. Math.* 2 (2016) 141–176.
- [55] J. Haubner, O. Hellan, M. Zeinhofer, M. Kuchta, Learning mesh motion techniques with application to fluid–structure interaction, *Comput. Methods Appl. Mech. Engrg.* 424 (2024) 116890, <http://dx.doi.org/10.1016/j.cma.2024.116890>, URL <https://www.sciencedirect.com/science/article/pii/S0045782524001464>.
- [56] P. Farrell, D. Ham, S. Funke, M. Rognes, Automated derivation of the adjoint of high-level transient finite element programs, *SIAM J. Sci. Comput.* 35 (4) (2013) C369 – C393.
- [57] A. Griewank, A. Walther, Algorithm 799: Revolve: An implementation of checkpointing for the reverse or adjoint mode of computational differentiation, *ACM Trans. Math. Software* 26 (2000) 19–45.
- [58] J.S. Dokken, S.K. Mitusch, S.W. Funke, Automatic shape derivatives for transient PDEs in FEniCS and Firedrake, 2020, arXiv preprint arXiv:2001.10058.
- [59] D.A. Ham, L. Mitchell, A. Paganini, F. Wechsung, Automated shape differentiation in the Unified Form Language, *Struct. Multidiscip. Optim.* 60 (5) (2019) 1813–1820.
- [60] T. Schwedes, S. Funke, D. Ham, An iteration count estimate for a mesh-dependent steepest descent method based on finite elements and Riesz inner product representation, 2016, arXiv e-print, <https://arxiv.org/abs/1606.08069>.
- [61] A. Wächter, L. Biegler, On the implementation of a primal-dual interior point filter line search algorithm for large-scale nonlinear programming, *Math. Program.* 106 (1) (2006) 25–57.
- [62] HSL, A collection of Fortran codes for large scale scientific computation, 2021, URL <https://www.hsl.rl.ac.uk/>. (Accessed April 2021).
- [63] P.R. Amestoy, A. Guermouche, J.-Y. L'Excellent, S. Pralet, Hybrid scheduling for the parallel solution of linear systems, *Parallel Comput.* 32 (2) (2006) 136–156.
- [64] S. Turek, J. Hron, Proposal for numerical benchmarking of fluid-structure interaction between an elastic object and laminar incompressible flow, in: H.-J. Bungartz, M. Schäfer (Eds.), *Fluid-Structure Interaction: Modelling, Simulation, Optimization*, in: *Lecture Notes in Computational Science and Engineering*, vol. 53, Springer-Verlag, Berlin, Heidelberg, 2006, pp. 371–385.
- [65] Q. Du, M. Gunzburger, L. Hou, J. Lee, Analysis of a linear fluid-structure interaction problem, *Discrete Contin. Dyn. Syst.* 9 (3) (2003) 633–650.
- [66] Q. Du, M. Gunzburger, L. Hou, J. Lee, Semidiscrete finite element approximation of a linear fluid-structure interaction problem, *SIAM J. Numer. Anal.* 42 (1) (2004) 1–29.
- [67] L. Failer, D. Meidner, B. Vexler, Optimal control of a linear unsteady fluid-structure interaction problem, *J. Optim. Theory Appl.* 170 (2016) 1–27.